AD-A039 092 IOWA UNIV IOWA CITY DEPT OF PHYSICS AND ASTRONOMY F/G 3/2
ION-ACOUSTIC WAVES IN THE SOLAR WIND.(U)
MAR 77 D A GURNETT, L A FRANK N00014-76-C-0016
UNCLASSIFIED U. OF IOWA-77-10 NL

1 OF 1
ADA039092

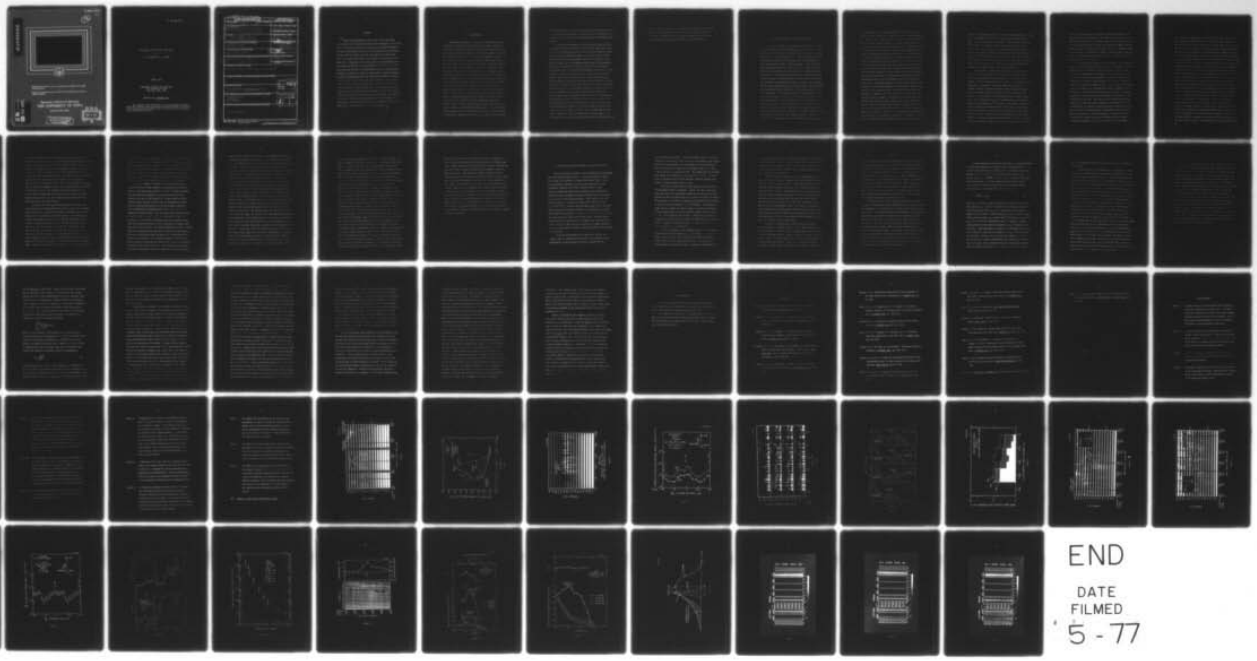

END
DATE FILMED
5-77

U. of Iowa 77-10

FG.

(12)

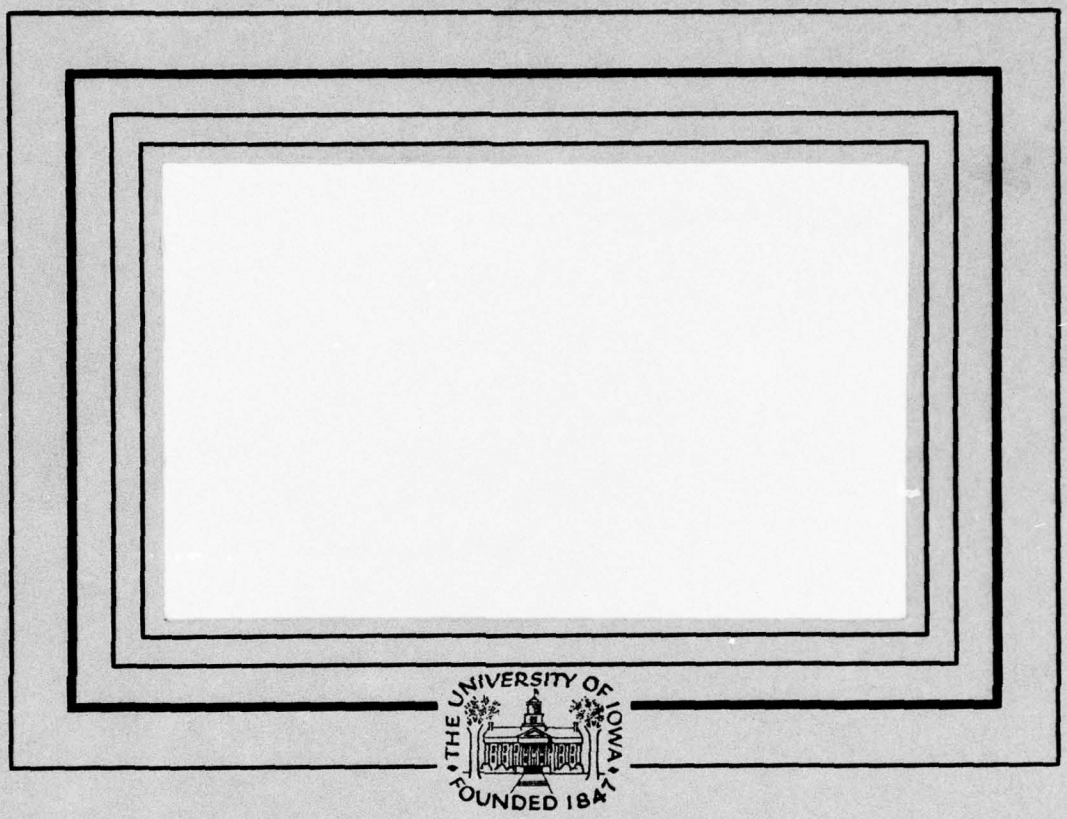

"Research was supported in part by the Office of Naval Research under Contract N00014-76-C-0016."

Department of Physics and Astronomy
THE UNIVERSITY OF IOWA
Iowa City, Iowa 52242

U. of Iowa 77-10

Ion-Acoustic Waves in the Solar Wind

by

D. A. Gurnett and L. A. Frank

March, 1977

Department of Physics and Astronomy
The University of Iowa
Iowa City, Iowa 52242

Submitted to J. Geophys. Res.

The research at the University of Iowa was supported in part by NASA under Contracts NAS5-11279, NAS5-11431 and NAS5-11064, and Grants NGL-16-001-002 and NGL-16-001-043 and by the Office of Naval Research under Grant N00014-76-C-0016.

UNCLASSIFIED

SECURITY CLASSIFICATION OF THIS PAGE (When Data Entered)

REPORT DOCUMENTATION PAGE

READ INSTRUCTIONS BEFORE COMPLETING FORM

1. REPORT NUMBER (14) U. of Iowa 77-10	2. GOVT ACCESSION NO.
3. RECIPIENT'S CATALOG NUMBER	
4. TITLE (and Subtitle) (6) Ion-Acoustic Waves in the Solar Wind.	5. TYPE OF REPORT & PERIOD COVERED: Progress, March 1977
	6. PERFORMING ORG. REPORT NUMBER
7. AUTHOR(s) (10) D. A. Gurnett and L. A. Frank	8. CONTRACT OR GRANT NUMBER(s): N00014-76-C-0016, (15) NASS-11279
9. PERFORMING ORGANIZATION NAME AND ADDRESS: Department of Physics and Astronomy, University of Iowa, Iowa City, IA 52242	10. PROGRAM ELEMENT, PROJECT, TASK AREA & WORK UNIT NUMBERS: (12) 66p.
11. CONTROLLING OFFICE NAME AND ADDRESS: Office of Naval Research, Arlington, Virginia (11)	12. REPORT DATE: Mar[redacted]77
	13. NUMBER OF PAGES: 64
14. MONITORING AGENCY NAME & ADDRESS (if different from Controlling Office) (9) Progress rept. 9	15. SECURITY CLASS. (of this report): UNCLASSIFIED
	15a. DECLASSIFICATION/DOWNGRADING SCHEDULE

16. DISTRIBUTION STATEMENT (of this Report)

Approved for public release; distribution is unlimited.

17. DISTRIBUTION STATEMENT (of the abstract entered in Block 20, if different from Report)

18. SUPPLEMENTARY NOTES

To be published in J. Geophys. Res., 1977.

19. KEY WORDS (Continue on reverse side if necessary and identify by block number)

Ion-acoustic waves
Solar wind
Wave Turbulence

20. ABSTRACT (Continue on reverse side if necessary and identify by block number)

[See page following]

ACCESSION for

NTIS	White Section ☑
DDC	Buff Section ☐
UNANNOUNCED	☐
JUSTIFICATION	
BY	
DISTRIBUTION/AVAILABILITY CODES	
Dist.	AVAIL. and/or SPECIAL
A	

DD FORM 1 JAN 73 1473 EDITION OF 1 NOV 65 IS OBSOLETE S/N 0102-014-6601

UNCLASSIFIED 188 460

SECURITY CLASSIFICATION OF THIS PAGE (When Data Entered)

ABSTRACT

Plasma wave measurements on the Helios 1 and 2 spacecraft have revealed the occurrence of electric field turbulence in the solar wind at frequencies between the electron and ion plasma frequencies. Wavelength measurements with the IMP 6 spacecraft now provide strong evidence that these waves are short wavelength ion-acoustic waves which are doppler shifted upward in frequency by the motion of the solar wind. Comparison of the Helios results with measurements from the earth-orbiting IMP 6 and 8 spacecraft shows that the ion-acoustic wave turbulence detected in interplanetary space has characteristics essentially identical to bursts of electrostatic turbulence generated by protons streaming into the solar wind from the earth's bow shock. In a few cases enhanced ion-acoustic wave intensities have been observed in direct association with abrupt increases in the anisotropy of the solar wind electron distribution. This relationship strongly suggests that the ion-acoustic waves detected by Helios far from the earth are produced by an electron heat flux instability, as suggested by Forslund. Possible related mechanisms which could explain the generation of ion-acoustic waves by protons streaming into the solar wind from the earth's bow shock are also considered.

I. INTRODUCTION

Plasma-wave measurements on the solar orbiting Helios 1 and 2 spacecraft [Gurnett and Anderson, 1977] have recently revealed the occurrence of significant levels of electric field turbulence in the solar wind at frequencies from about 1 to 10 kHz, between the electron and ion plasma frequencies. In this paper we expand the initial investigation of this turbulence and present evidence that this turbulence consists of ion-acoustic waves below the ion plasma frequency which are doppler shifted upward in frequency by the motion of the solar wind. Measurements are presented both in interplanetary space, from Helios 1 and 2, and in the solar wind upstream of the earth's bow shock, from IMP 6 and 8. These data provide a comprehensive description of the spectrum, polarization, wavelength and other essential characteristics of the turbulence. Comparisons are also made with the ambient plasma parameters under a variety of conditions to identify the origin of these waves. In interplanetary space, far away from the earth, the primary mechanism for producing the ion-acoustic waves is believed to be the electron heat flux instability suggested by Forslund [1970]. Near the earth, however, the same type of waves are often observed to be associated with low-energy, 1 to 10 keV, protons streaming toward the sun from the earth's bow shock. Thus, more than one mechanism is apparently operative in the solar wind to destabilize

the ion-acoustic mode. As will be discussed, similar mechanisms, based on an induced drift between the solar wind electrons and protons, are believed to account for both the heat flux and proton streaming instabilities.

In the initial description of the ion-acoustic wave turbulence by Gurnett and Anderson [1977] this turbulence was called $f_p^+ < f < f_p^-$ noise. This terminology was chosen on a strictly observational basis, since the largest intensities usually occur in the frequency range between the electron and ion plasma frequencies, f_p^- and f_p^+. As detected by Helios 1 and 2 the maximum single channel ($\pm$ 10% bandwidth) electric field amplitudes of the $f_p^+ < f < f_p^-$ noise are typically a few hundred $\mu V\ m^{-1}$. The electric field strength of this noise is very impulsive, consisting of many brief bursts lasting for only a few seconds. When viewed on a time scale of several hours or more the $f_p^+ < f < f_p^-$ noise is present a large fraction (30 to 50%) of the time. The noise is observed over the entire range of the Helios orbits from about 0.3 to 1.0 A.U. The frequency spectrum of the $f_p^+ < f < f_p^-$ noise shows a systematic variation with radial distance from the sun, shifting toward higher frequencies closer to the sun. Spin modulation measurements show that the electric field of the noise tends to be aligned along the direction of the magnetic field in the solar wind. Gurnett and Anderson discussed the possible plasma wave modes which could account for the $f_p^+ < f < f_p^-$ noise and concluded that the noise could be produced by either the Buneman mode [Buneman, 1958] or by the ion-acoustic mode, with the ion-acoustic mode being the most likely.

Since the $f_p^+ < f < f_p^-$ noise is now definitely believed to be associated with the ion-acoustic mode, we will consistently refer to this noise as "ion-acoustic waves", even though the detailed arguments for this identification are presented in a later section of this paper.

II. HELIOS OBSERVATIONS IN INTERPLANETARY SPACE

Since more data have now been analyzed from the Helios plasma wave experiments, a much more detailed analysis of the ion-acoustic waves detected by Helios in the interplanetary medium can be provided than was given in the initial survey by Gurnett and Anderson [1977]. For details of the Helios 1 and 2 plasma wave instrumentation see Gurnett and Anderson [1977]. A typical example of the ion-acoustic waves detected by Helios 2 is shown in Figure 1. Helios 2 at this time is near the earth-sun line at a heliocentric radial distance of about 0.45 A.U. These data are selected from a period when a nearly continuous level of ion-acoustic wave turbulence was being detected. The solid lines for each frequency channel in Figure 1 show the peak electric field intensities over 40.0 second intervals and the vertical bars (solid black areas) indicate the corresponding average electric field intensities. The intensity scales are logarithmic with a total range of 100 db from the bottom of one channel to the bottom of the next adjacent channel. The ion-acoustic turbulence is evident as a broad band of noise extending from about 1.0 to 17.8 kHz, roughly between the electron and ion plasma frequencies, f_p^- and f_p^+, as indicated on the right-hand side of Figure 1. A typical spectrum, selected from Figure 1 at a time of nearly maximum intensity is shown in Figure 2. The broad peak in the spectrum between the electron and

ion plasma frequencies is clearly evident. As will be discussed later, the relationship to the local electron and ion plasma frequencies, $f_p^+ < f < f_p^-$, is mainly fortuitous, since the frequency spectrum of the ion-acoustic wave turbulence is strongly doppler shifted by the motion of the solar wind. Both Figures 1 and 2 show that the peak field strengths of the ion-acoustic waves are much larger than the average field strengths, indicating that the noise is very impulsive. The detailed temporal variations are illustrated in Figure 3, which shows a very high time resolution snapshot of the electric field intensities stored in the spacecraft memory from the event in Figure 1, at about 0257 UT. These high time resolution measurements show that the ion-acoustic turbulence consists of many short bursts lasting only a few tenths of a second. The individual bursts have a very broad bandwidth and tend to occur simultaneously across a broad range of frequencies. Occasionally high time resolution measurements, such as in Figure 3, show distinct evidence of spin modulation caused by the rotation of the electric antenna. A brief period where such spin modulation is apparent occurs from about +12 to +15 seconds in the 1.78 kHz channel in Figure 3. The spin modulation consists of two maxima and two minima in each 1 second rotation of the spacecraft. In most cases, the extremely rapid temporal variations make it very difficult to accurately determine the phase of the spin modulation. However, by averaging a long series of measurements the detailed spin modulation pattern can usually be identified. An example of one such series of measurements is illustrated in Figure 4, which shows the

electric field intensity distribution above a fixed percentage occurrence level (10 and 20%) as a function of the antenna orientation angle ϕ_{SE}^{A}. A long, 1-hour, analysis interval is used to reduce statistical fluctuations. These data show that the maximum electric field intensity occurs when the antenna is oriented approximately parallel to the solar wind magnetic field. Individual high time resolution measurements of the spin modulation, as in Figure 3, also show this same relationship. From these measurements it is concluded that the electric field of the ion-acoustic wave turbulence is oriented approximately parallel to the static magnetic field in the solar wind.

To illustrate the approximate fraction of the time that the ion-acoustic wave turbulence is present in the solar wind, Figure 5 shows the peak and average field strengths for one complete solar rotation. The four frequencies shown in Figure 5 are selected to cover the range of frequencies in which the ion-acoustic turbulence is normally observed. The peak and average field strengths are shown by lines and vertical bars, as in Figure 1. A time interval of 36.0 minutes is used for both the peak and average field strength calculations. It is evident from Figure 5 that peak electric field amplitudes of a few hundred $\mu V\ m^{-1}$ are present in the frequency range from 1.78 to 5.62 kHz a substantial fraction of the time. Occasionally bursts of ion-acoustic noise are seen to extend into the 562 Hz and 17.8 kHz channels. Because of the long interval for the peak determination, the compressed time scale presentation in Figure 5 tends to enhance the apparent occurrence of ion-acoustic waves, since even one

short burst during any given 36 minute interval will register in the peak measurements. Nevertheless, these data show that bursts of ion-acoustic wave turbulence are a common feature of the solar wind, since during any given 36 minute interval a few bursts are normally detected. Occasionally quiet periods occur, such as on Oct. 20. However, usually some turbulence is detected in any given 36 minute interval. Sometimes distinct enhancements are evident for periods of several days, as for example from Oct. 7 to Oct. 12.

To investigate the variation in the spectrum of the ion-acoustic wave turbulence with radial distance from the sun a detailed statistical analysis has been performed on all of the available Helios 1 data, consisting of approximately two complete orbits around the sun. The results of this analysis are summarized in Figure 6, which shows the distribution of electric field strengths detected in each frequency channel as a function of radial distance. The electric field strengths used in this analysis are 36 minute peak values, comparable to those in Figure 5. The electric field strength contours shown in Figure 6 correspond to intensities which are exceeded a fixed fraction (5 and 10 percent) of the time. The portion of the overall spectrum attributed to the ion-acoustic wave turbulence is indicated by the cross-hatched areas. The steeply rising spectrum at low frequencies, $\leq$ 500 Hz, is caused by interference from the spacecraft solar array (also evident in Figure 1). The isolated peaks in the spectrum at high frequencies, $\geq$ 30 kHz, are caused by narrowband electron plasma oscillations comparable to the event in Figure 1 at about 0700 UT.

These plasma oscillations are directly associated with energetic electrons streaming outward from the sun [Gurnett and Frank, 1975] and are often directly associated with type III solar radio bursts [Gurnett and Anderson, 1976]. Although narrowband electron plasma oscillations are easily distinguished from ion-acoustic waves, no attempt was made to separate the two types of waves for the statistical analysis in Figure 6 since the plasma oscillations occur very infrequently. Figure 6 clearly shows that both the frequency and intensity of the ion-acoustic waves increase with decreasing radial distance from the sun. A rough analysis indicates that the frequencies of both the ion-acoustic waves and the electron plasma oscillations vary approximately as $1/R$, where R is the heliocentric radial distance. The radial variation of the ion-acoustic wave intensity is shown in more detail by Figure 7, which gives the distribution of broad-band electric field strengths as a function of the radial distance from the sun. The broad-band electric field strengths used in this analysis are calculated by integrating the individual, 36 minute, peak electric field spectrums from 562 Hz to 31.1 kHz. As can be seen from Figure 6, the main part of the ion-acoustic wave spectrum usually occurs in this frequency range. The frequency of occurrence contours in Figure 7 clearly show the increase in the ion-acoustic wave intensity with decreasing radial distance from the sun. A best fit analysis of the broad band field strength as a function of the radial distance, assuming a power law radial distance dependence, indicates that the electric field strength also varies approximately as $1/R$.

III. IMP 6 AND 8 OBSERVATIONS UPSTREAM OF THE EARTH'S BOW SHOCK

Waves essentially identical to the ion-acoustic waves detected by Helios are also commonly observed by the IMP 6 and 8 spacecraft in the solar wind upstream of the earth's bow shock. See Gurnett [1974] for a description of the plasma wave instrumentation on IMP 6 and 8. As will be shown, some of the ion-acoustic waves detected by IMP 6 and 8 are clearly of terrestrial origin, whereas others appear to be of interplanetary origin, as in the Helios observations. Figures 8, 9 and 10 illustrate some typical examples of the ion-acoustic waves detected by IMP 8 upstream of the bow shock. Figure 8 shows an example of an earth-related event in which a burst of ion-acoustic waves, from about 0920 to 1115 UT, is closely associated with the arrival of a stream of low-energy protons from the earth's bow shock. The corresponding charged particle measurements from the University of Iowa low-energy-proton-electron-differential-energy-analyzer (LEPEDEA) on IMP 8 are shown in Plate 1. Details of this spectrogram display of the charged particle intensities and the LEPEDEA instrumentation are given by Frank et al. [1976]. The sunward streaming 1 to 10 keV protons associated with the ion-acoustic waves are clearly evident in the second, third and fourth spectrograms from the top in Plate 1, between about 0920 and 1115 UT, in almost exact coincidence with the burst of ion-acoustic waves. These spectrograms represent viewing directions looking toward

local evening, local midnight, and local morning, respectively. The direction of motion of the protons can also be seen from the sector spectrogram in Plate 1, which shows that the protons are streaming toward the sun with directions of arrival in the range $120° \leq \varphi^{L}_{SE} \leq 300°$ (solar ecliptic coordinates). IMP 8 at this time is located upstream of the earth, at a local time of about 14.5 hr. and a geocentric radial distance of about 41 R_e. The observed directions of arrival correspond closely with the expected directions of motion for particles originating from the vicinity of the earth. The velocity distribution function for these protons, measured along directions approximately parallel to the earth-sun line is shown in Figure 11, along with the ambient solar wind distribution determined from the Los Alamos plasma instrument on IMP 8 [personal communication, W. Feldman]. As can be seen from Figure 11, the protons streaming into the solar wind produce a very pronounced double peak in the proton distribution function. Possible mechanisms by which these sunward streaming protons can generate ion-acoustic waves are considered later.

Upstream ion-acoustic waves associated with sunward streaming protons, such as illustrated in Figure 8, almost certainly correspond to the electrostatic noise first reported by Scarf et al. [1970] using measurements from OGO 5. In comparison to the ion acoustic waves detected by Helios, the upstream waves detected by IMP 8 have essentially identical characteristics. In both cases the noise is electrostatic and extends with comparable intensities from about 562 Hz to 10 kHz, between the electron and ion plasma frequencies. The peak

electric field strengths are much greater than the average electric field strengths, as in the Helios measurements, and angular distributions, such as in Figure 12, show that the wave electric field is aligned approximately parallel to the solar wind magnetic field, also in agreement with the Helios observations. From all available evidence, the electrostatic waves generated upstream of the earth by protons arriving from the bow shock are essentially identical to the ion-acoustic waves detected by Helios far from the earth. These comparisons indicate that the same basic plasma wave mode, the ion-acoustic mode, is involved in both types of noise. The detailed mechanisms by which the ion-acoustic waves are generated must, however, be quite different, since protons from the earth's bow shock cannot possibly produce the waves detected by Helios far from the earth.

Not all of the ion-acoustic waves detected by IMP 8 are associated with protons arriving from the bow shock. Figure 9, for example, shows a sequence of ion-acoustic wave events extending over an entire day which are not related to upstreaming protons. The corresponding LEPEDEA spectrograms in Plate 2 for the same day demonstrate that no sunward streaming protons are detectable during these events, except possibly for the event around 1300 to 1400 UT. The magnetic field during this day is often close to the ecliptic plane, so there is no possibility that the LEPEDEA, which scans viewing directions in the ecliptic plane, would not be able to detect protons streaming along the magnetic field from the bow shock. The corresponding electron spectrograms in Plate 2 also show no abrupt changes in the electron distribution

function which can be clearly related to variations in the ion-acoustic wave intensity. Ion-acoustic wave activity of this type, for which no earth-related source can be identified, constitutes about 30 to 50% of all of the ion-acoustic wave activity detected by IMP 8 upstream of the bow shock. Events of this type evidently correspond to the interplanetary ion-acoustic wave turbulence commonly detected by Helios far from the earth, since no earth-related source can be identified.

To try to identify the feature of the solar wind charged-particle distribution which produces the interplanetary (non-earth related) ion-acoustic wave turbulence, the IMP 8 LEPEDEA and plasma wave data have been examined for correlated events which would indicate the origin of the instability. Several events have been identified which strongly indicate that the anisotropy associated with the electron heat flux in the solar wind plays an important role in producing the ion-acoustic wave turbulence, as was first suggested by Forslund [1970]. One such event, which occurred during a disturbed period on July 5, 1974, is illustrated in Figure 10 and Plate 3. In this case a pronounced burst of ion-acoustic turbulence occurs from about 1645 to 1930 UT, preceded by a shorter burst from about 1540 to 1600 UT. The LEPEDEA spectrograms in Plate 3 clearly show that no protons are arriving from the earth's bow shock during this time, so these waves must correspond to the interplanetary ion-acoustic wave turbulence. The enhanced background, evident in the proton spectrogram throughout the period shown in Plate 3, is caused by an energetic solar cosmic ray event. Close examination of the electron sector spectrogram in the second panel from the bottom in Plate 3

shows that the ion-acoustic turbulence occurs during a period when a substantial anisotropy is present in the solar wind electron distribution. The maximum intensities occur for LEPEDEA viewing directions in the range $0° \leq \varphi^{L}_{SE} \leq 90°$, which are approximately symmetrical with respect to the magnetic field direction, $\varphi^{B}_{SE} \simeq 45°$, during this period. This anisotropy is representative of a substantial streaming of electrons along the magnetic field away from the sun. The electron velocity distribution indicates that these electrons correspond to the high temperature "halo" electrons which provide the main contribution to the heat flux in the solar wind [Feldman et al., 1974]. The anisotropy evident in Plate 3 corresponds to an unusually large electron heat flux away from the sun, directed along the solar wind magnetic field. The detailed variations of the electron velocity distribution function at a fixed energy and the corresponding 1.78 kHz electric field intensity variations are shown in Figure 13 near the beginning of the event. The electron distribution function is shown in two directions, $\varphi^{L}_{SE} = 34°$ and 124°, which are approximately parallel and perpendicular to the average magnetic field directions projected onto the ecliptic plane during this period. The interpretation of these data is somewhat complicated by variations in the magnetic field direction. Before about 1610 UT the magnetic field is too far out of the ecliptic plane, $\theta^{B}_{SE} \geq 60°$, for accurate measurements of the anisotropy, parallel and perpendicular to the magnetic field. However, after about 1610 UT the magnetic field is sufficiently close to the ecliptic plane, $\theta^{B}_{SE} \leq 30°$, for good anisotropy measurements. As can

be seen from Figure 13, after about 1650 the intensities at $\varphi^L_{SE} = 34°$, along the magnetic field looking toward the sun, increase substantially above the intensities at $\varphi^L_{SE} = 124°$, perpendicular to the magnetic field. Comparisons with the 1.78 kHz electric field intensities show that the onset of the ion-acoustic turbulence is closely correlated with the increase in the anisotropy of the electron distribution. The burst of noise at about 1550 UT is also seen to be closely correlated with the increase of electron intensities in the direction $\varphi^L_{SE} \simeq 34°$ at about 1552 UT. Even though θ^B_{SE} is large at this time this burst must be associated with an anisotropic component streaming along the magnetic field since the intensity perpendicular to the magnetic field, $\varphi^L_{SE} = 124°$, shows no comparable increase. The evidence that the ion-acoustic wave turbulence is associated with the magnetic-field-aligned anisotropy in the electron flux is further supported by the velocity distributions shown in Figure 14, which are selected for times when $\theta^B_{SE} \simeq 0°$ and for viewing directions parallel ($\varphi^L_{SE} = 304°$ and 34°) and anti-parallel ($\varphi^L_{SE} = 124°$ and 214°) to the magnetic field. The electron intensity measurements at 1252 UT (triangles), before the onset of the ion-acoustic wave turbulence, shows that the anisotropy is typically small, $\leq 20\%$, at all velocities. However, the measurements at 1720 UT (circles), after the onset of the ion-acoustic wave turbulence, show that the anisotropy is very large, typically a factor of 3 to 5, over a broad range of velocities. These velocity distributions also show that, other than the change in the anisotropy, the electron distribution functions are nearly identical in the two regions, before

and after the onset of the ion-acoustic turbulence. Comparison of these velocity distributions with the measurements of Feldman et al. [1975] clearly identifies this anisotropy with a greatly enhanced heat flux of the halo electrons, directed along the magnetic field line away from the sun. These and other similar observations provide strong evidence that the anisotropy associated with the electron heat flux in the solar wind plays an essential role in the generation of these waves. Close inspection of the electron angular distributions in Plate 2 also shows, for example, that a similar electron anisotropy is present during the period when the ion-acoustic waves in Figure 9 are being observed. The variations in the ion-acoustic wave intensity are not, however, as easily associated with changes in the electron distribution function in this case, possibly because the ion-acoustic mode is close to marginal stability, so that only very minor changes in the electron distribution or other parameters can trigger the growth or decay of the waves.

IV. IDENTIFICATION OF THE TURBULENCE AS ION-ACOUSTIC WAVES

Some of the factors involved in the identification of the plasma wave mode associated with the $f_p^+ < f < f_p^-$ noise detected by Helios have already been discussed by Gurnett and Anderson [1977]. From the electrostatic character of the noise and the electric field orientation (parallel to the static magnetic field), a wide variety of plasma wave modes can be eliminated from consideration. Essentially only two plasma wave modes are known which could account for all of the observed characteristics. These modes are the ion-acoustic mode at $f \lesssim f_p^+$ and the Buneman mode [Buneman, 1958] at $f_B \simeq (m^-/m^+)^{1/3} f_p^-$. We also note that Scarf et al. [1970] identified these same modes as the best candidates for explaining the upstream electrostatic noise, which is now believed to be the same basic plasma wave mode detected by Helios far from the earth. Although Gurnett and Anderson [1977] argue that it is unlikely that the proper conditions exist in the solar wind for generating the Buneman instability no method was available to clearly distinguish between these two modes of propagation.

One way of distinguishing the Buneman mode from the ion-acoustic mode is to measure the wavelength. The two modes differ fundamentally in the wavelengths required to account for the

observed frequency spectrums. Since ion acoustic waves only occur at frequencies less than f_p^+ in the rest frame of the plasma, large doppler shifts and correspondingly short wavelengths of tens to hundreds of meters are required to account for the frequency range, $(2 - 10)f_p^+$, in which the noise is usually observed. The Buneman mode, on the other hand, occurs at a frequency, $f_B \simeq 3.49\, f_p^+$, which requires no doppler shift to account for the observed frequency spectrum, implying wavelengths of several hundred meters or more.

Since only a single electric dipole antenna is used on Helios, the wavelength cannot be determined. However, the IMP 6 spacecraft, which also detects the same waves upstream of the bow shock, has two antennas of different lengths which can be used to estimate wavelengths. The technique used consists of comparing the measured antenna voltages, V, with the tip-to-tip lengths, L, of the antennas. For wavelengths longer than the antenna the antenna voltage is directly proportional to the antenna length, so that the computed electric field strength, $E = 2V/L$, is the same for both antennas. However, for wavelengths, λ, comparable or shorter than the antenna this proportionality no longer holds. In general we expect that when $\lambda \leq L$ the measured electric field strength will be underestimated.

On IMP 6 the electric field antennas consist of two orthogonal dipoles with tip-to-tip lengths of $L_y = 92.5$ meters and $L_x = 53.5$ meters [Gurnett, 1974]. The two antennas are mounted orthogonally to each other and to the spacecraft spin axis. The spin axis is directed normal to the ecliptic plane. Simultaneous measurements of

the voltage spectrums from the two antennas are made with two identical spectrum analyzers. Because of their orientation the two antennas do not detect the same component of the electric field. However, for a steady-state wave spectrum comparisons can be made by averaging over many rotations of the spacecraft.

A case for which the wavelength of the interplanetary ion-acoustic turbulence has been estimated using this technique is shown in Figure 15. During this period IMP 6 is upstream of the bow shock at geocentric radial distances from about 19 to 26 R_e and local times from about 9.8 to 10.2 hr. A substantial level of ion-acoustic wave activity is present during this period. Some of these events can be associated with low-energy protons arriving from the bow shock, whereas other events, such as the intense burst from about 0520 to 0610 UT, are of interplanetary origin. This period of enhanced ion-acoustic wave activity occurs shortly after an abrupt increase in the solar wind density at about 0500 UT (see the top panel of Figure 15), which preceded the onset of a high-speed solar wind stream a few hours later [W. Feldman, personal communication].

The electric field spectrums obtained from the E_y and E_x antennas during the interval from about 0530 to 0602 UT are shown in the bottom panel of Figure 16. These spectrums give the median values of all of the peak intensities obtained during this interval, computed using $E = 2V/L$. Each point represents the median of approximately 700 individual peak measurements. Because of the impulsive temporal fluctuations a large number of measurements are needed to reduce the

statistical fluctuations to an acceptable level. The ratio of the E_y to the E_x field strengths, computed from these spectrums, is shown in the top panel of Figure 16, with estimates of the corresponding error limits (one standard deviation). As can be seen the E_y/E_x ratio is approximately one at low frequencies, $f \leq 3$ kHz, but deviates substantially below one at high frequencies, $f \geq 10$ kHz. The decrease in the E_y/E_x ratio at high frequencies indicates that the longer, E_y, antenna is significantly underestimating the field strengths in comparison to the shorter, E_x, antenna. This deviation of the E_y/E_x ratio indicates that wavelengths shorter than $L_y = 92.5$ meters are being detected at frequencies above about 3 kHz.

To demonstrate the overall accuracy and reliability of this technique a corresponding analysis was performed on a band of whistler-mode plasmaspheric hiss detected in the earth's magnetosphere a few hours later. It is easily shown that the wavelengths of these whistler-mode waves are very large, much larger than the dimensions of the IMP-6 electric antennas. The results of this analysis are shown in Figure 17. As can be seen the E_y/E_x ratio stays very close to one at all frequencies, thereby confirming that the wavelengths are longer than the antenna length. These and many other similar comparisons for a wide variety of plasma wave phenomena demonstrate that significant deviations of the E_y/E_x ratio below one, such as in Figure 16, are not instrumental effects and can only be attributed to wavelengths shorter than the antenna length.

Having confirmed the accuracy of the method, it is now of interest to compare the measurements in Figure 16 with the wavelengths to be expected if the waves are ion-acoustic waves. For typical solar wind parameters, $T^- \simeq 1.5 \times 10^5$ °K, it is readily shown that the ion-acoustic speed, $C_s = \sqrt{kT^-/m^+} \simeq 35.2$ km $(sec)^{-1}$, is much less than the solar wind velocity. For these conditions the frequency detected in the spacecraft frame of reference is, to a good approximation, given entirely by the doppler shift (valid for $f \gg f_p^+$),

$$f = \left(\frac{V_{SW}}{\lambda}\right) \text{Cos } \theta_{kV} \ , \qquad (1)$$

where θ_{kV} is the angle between the propagation vector $\vec{k}$ and the solar wind velocity, $\vec{V}_{SW}$. Since the electric field and $\vec{k}$ are parallel to the solar wind magnetic field, θ_{kV} can be determined from the measured magnetic field direction. Solving equation (1) for λ, using the appropriate solar wind speed, $V_{SW} \simeq 360$ km $(sec)^{-1}$ from Figure 15, and using $\theta_{kV} \simeq 22°$ from the IMP 6 magnetometer data [D. Fairfield, personal communication] the wavelengths corresponding to each frequency can be calculated. These wavelengths are shown by the wavelength scale at the top of Figure 16, along with the lengths, L_y and L_x, of the two electric antennas. As can be seen, the E_y/E_x ratio starts to deviate below one as soon as the computed wavelength becomes significantly shorter than the antenna. These comparisons show that the wavelength computed from the doppler shift formula is in excellent quantitative agreement

with the wavelength estimated from the E_x/E_y ratio ($\lambda \simeq 92.5$ meters at $f \simeq 3$ kHz).

Further evidence of short wavelengths is provided by the upper cutoff of the observed frequency spectrum and the variation of this cutoff with radial distance from the sun. It is well known that the shortest wavelength which can occur in a plasma is determined by the onset of strong Landau damping at a wavelength of about $2\pi \lambda_D$, where $\lambda_D^2 = \epsilon_o kT/ne^2$ is the Debye length. The minimum wavelength, $\lambda_{min} = 2\pi \lambda_D$, computed from the measured plasma density, $n \simeq 35$ $(cm)^{-3}$, and temperature, $T^- = 1.4 \times 10^5$ °K, is approximately 27.5 meters, as shown at the top of Figure 16. As can be seen, this minimum wavelength is in excellent agreement with the observed upper cutoff frequency of the electric field spectrum. The dependence of the minimum wavelength on the plasma density, $\lambda_{min} \propto \lambda_D \propto 1/\sqrt{n}$, furthermore explains the tendency for the upper cutoff frequency, $f_{max} \simeq (V_{SW}/\lambda_{min}) \propto \sqrt{n}$, to increase with decreasing radial distance from the sun (see Figure 6), since the plasma density increases closer to the sun. Using the plasma density scaling law, $n \propto 1/R^2$, appropriate for the solar wind far from the sun, the upper cutoff frequency should vary approximately as $f_{max} \propto 1/R$, which is seen to be in good agreement with the observed radial variation of the upper cutoff frequency illustrated in Figure 6. These comparisons all provide strong evidence that the low frequency electrostatic waves detected in the solar wind by IMP 6, IMP 8 and Helios have short wavelengths and doppler shifts consistent with the identification of these waves as ion-acoustic waves.

Although short wavelengths are clearly evident for the event in Figure 16, in most cases ion-acoustic waves detected by IMP 6 do not show these effects. The event in Figure 16 is unusual in that the plasma density is very large, $n = 35\ (cm)^{-3}$, which results in a minimum wavelength substantially less than the antenna length. For typical solar wind plasma densities at 1 A.U., $n \simeq 5\ (cm)^{-3}$, the minimum wavelength is approximately $\lambda_m = 72$ meters, which is evidently sufficiently large to make short wavelength effects undetectable even though wavelengths shorter than the IMP 6 antenna length, $L_y = 92.5$ meters, could occur. Note from Figure 16 that most of the wave energy occurs at wavelengths substantially larger than $\lambda_{min} = 2\pi\lambda_D$ and that the intensity is strongly attenuated for wavelengths approaching λ_{min}. It should also be noted that because of the shorter length of the Helios antennas (L = 16 meters for Helios 1 and L = 32 meters for Helios 2), errors due to short wavelength effects are not normally expected to be significant for the Helios measurements, except for unusually high densities.

V. SUMMARY AND DISCUSSION

Plasma wave measurements on the solar orbiting Helios spacecraft have previously shown that sporadic bursts of electrostatic turbulence are commonly observed in the solar wind at frequencies between the electron and ion plasma frequencies [Gurnett and Anderson, 1977]. In this paper we have expanded the earlier investigation of these waves using the Helios data and have compared the Helios results with similar measurements from the earth-orbiting IMP 6 and 8 spacecraft. Wavelength measurements with the IMP 6 spacecraft now provide strong evidence that these waves are short wavelength ion-acoustic waves at $f \leq f_p^+$ which are doppler-shifted upwards in frequency by the motion of the solar wind. The upper cutoff frequency, and the variation of this cutoff frequency with radial distance from the sun, $f_{max} \propto 1/R$, are in close agreement with the short wavelength cutoff expected for ion-acoustic waves.

Comparison with the IMP 6 and 8 data reveal that a substantial fraction, 50 to 70%, of the ion-acoustic wave turbulence detected in the solar wind near the earth is caused by suprathermal protons streaming into the solar wind from the earth's bow shock. These waves, which correspond to the upstream electrostatic waves first reported by Scarf et al. [1970], are observationally indistinguishable from the ion-acoustic waves detected by Helios. Although the upstream proton-

driven waves and the waves detected by Helios are both evidently ion-acoustic waves, some distinctly different source is required to explain the Helios observations, since protons from the earth's bow shock cannot possibly account for the waves detected by Helios far from the earth. Examination of the IMP 6 and 8 data reveals many examples of ion-acoustic turbulence during periods when no protons can be detected coming from the earth's bow shock. These events evidently correspond to the waves detected by Helios far from the earth. Usually in these cases there is no evidence of significant suprathermal electron or proton fluxes, other than the quiescent solar wind distribution. In a few events variations in the ion-acoustic wave intensity were found which are closely correlated with changes in the anisotropy of the solar wind electron distribution. These events strongly suggest that the ion-acoustic turbulence is driven by the anisotropy associated with the electron heat flux in the solar wind, as suggested by Forslund [1970].

The basic mechanism proposed by Forslund [1970] is illustrated schematically in Figure 18, which shows the general form of the reduced one-dimensional electron and proton distribution functions in the solar wind. The reduced one-dimensional distribution functions are computed from $F(V) = \int d\vec{V}_\perp f(\vec{V})$, where $f(\vec{V})$ is the three-dimensional distribution function and $d\vec{V}_\perp$ represents an integration over velocities perpendicular to the magnetic field. As indicated, a substantial anisotropy is produced in the high energy, or "halo", electrons by the electron heat flux flowing outward away from the

sun [Feldman et al., 1974, 1975]. Since the net current in the solar wind is essentially zero, except at discontinuities, the electron current associated with the antisunward drift of the energetic "halo" electrons must be compensated by a sunward drift of the low-energy "core" electrons. This drift velocity, V_d, is indicated in Figure 18. If the double peak in the combined velocity distribution function, $F(V) = F^-(V) + (m^-/m^+)\, F^+(V)$, produced by this drift is sufficiently large then the ion-acoustic mode is unstable. The condition for instability is given by the Penrose criterion

$$\int_{-\infty}^{\infty} \frac{F(V)-F(V_o)}{(V-V_o)^2}\, dV > 0 \ , \qquad (2)$$

where V_o is the velocity of the minimum in $F(V)$ [Penrose, 1960]. For equal electron and ion temperatures, $T^- \simeq T^+$, the threshold drift velocity is very large, approximately $V_t = \sqrt{kT^-/m^-}$, which is too large to be exceeded in the solar wind. However, if $T^- \gg T^+$, which is sometimes satisfied in the solar wind, then the threshold drift velocity for instability is greatly reduced, to approximately

$$V_t \simeq \sqrt{\frac{kT^+}{m^+}} \qquad (3)$$

[Krall and Trivelpiece, 1973]. For a solar wind ion temperature of $T^+ \simeq 4.0 \times 10^4$ °K, the threshold drift velocity is, for example, only $V_t = 18$ km $(\text{sec})^{-1}$ (assuming $T^- \gg T^+$). For electron temperatures only moderately larger than the ion temperature the threshold drift velocity

is larger than equation (3), by a factor which depends on T^-/T^+ [see Krall and Trivelpiece, 1973]. Based on his analysis, Forslund [1970] concluded that the ion-acoustic mode should be driven unstable by the electron heat flux whenever the electron to ion temperature ratio is sufficiently large.

Although the observations of an association between the anisotropy in the electron distribution function and the occurrence of ion-acoustic waves provide strong evidence for the mechanism proposed by Forslund [1970], the detailed arguments in support of this mechanism are more involved, since all other types of double peaked distribution functions which could possibly generate ion-acoustic waves must be eliminated from consideration. Charged particle measurements such as in Plates 2 and 3 clearly show that ion-acoustic waves occur during times when no secondary peak is detectable in either the electron or proton distribution functions, within the energy range, 50 eV $\leq$ E $\leq$ 45 keV, and resolution of the LEPEDEA. Although electron energies less than 100 eV were not investigated, it is almost completely certain, based on the results of Feldman et al. [1975], that double peaks do not occur in the electron distribution function at energies less than 100 eV. It is possible that closely spaced double peaks could occur in the ion distribution, such as the double proton streams reported by Feldman et al. [1973a], and still be unresolved in the LEPEDEA data. Comparisons with published examples of double proton streams [Feldman et al., 1973a] do not show a close correspondence with the occurrence of ion-acoustic waves, however, further detailed studies are needed to investigate whether double proton streams can under some

circumstances generate ion-acoustic waves. Since neither the electron nor ion distribution functions apparently have the double-peaked form required to produce an instability, essentially the only possibility left is the double peak produced by a velocity shift between the peaks in the electron and ion distributions, as illustrated in Figure 18. The presence of such a velocity shift in the solar wind has now been amply demonstrated by Feldman et al. [1974, 1975]. It only remains to be demonstrated that this shift is sufficiently large to exceed the threshold for generating ion-acoustic waves. The magnitude of the velocity shift, which is difficult to measure directly, can be estimated from the anisotropy in the halo electron distribution. For the event in Figure 14 at 1720 UT, the flux of electrons along the magnetic field (first moment) is estimated to be 1.50×10^8 electrons $(cm^2\text{-sec})^{-1}$. Using the measured local plasma density of $n = 10.1$ $(cm)^{-3}$, this flux must be compensated by a sunward drift of the core electrons at a velocity of about 150 km $(sec)^{-1}$. The ratio of this drift velocity to the electron thermal speed (using $T^- = 1.5 \times 10^5$ °K) is about 0.1. Whether this drift velocity exceeds the threshold drift velocity for the ion-acoustic wave instability is critically dependent on the electron to ion temperature ratio. For the period of interest the ion temperature measured by the Los Alamos plasma probe on IMP 8 is $T^+ = 7.1 \times 10^4$ °K. Using a typical temperature of $T^- = 1.5 \times 10^5$ °K for the core electrons the temperature ratio is $T^-/T^+ = 2.14$. For this relatively low electron to ion temperature ratio the ion-acoustic mode should be stable according to the curves given by Stringer [1964]. On the other hand, if a typical halo temperature of $T^- = 7.0 \times 10^5$ °K

is used, which gives $T^-/T^+ = 10$, the threshold drift velocity given by equation (3), $V_t = 23$ km $(sec)^{-1}$, valid when $T^- \gg T^+$, is exceeded by a substantial factor. Since no computer calculations of the threshold drift velocity are available for a realistic combination of core and halo electron distributions, the stability of the ion-acoustic mode cannot be accurately determined. However, since the correct effective electron to ion temperature ratio is probably somewhere in between the two extremes given by the core and halo temperatures, it seems likely that the ion-acoustic mode is unstable in this case. Further detailed analyses of the exact instability conditions are needed for realistic models of the solar wind electron distribution to clearly answer this question.

For the ion-acoustic waves generated by protons streaming into the solar wind from the bow shock there is no question about which particles are responsible for the instability. However, considerable uncertainty still remains concerning the detailed mechanism by which the proton stream produces the instability. In considering the origin of the instability two distinctly different mechanisms can be identified: (1) the instability may be caused directly by the double peak in the proton distribution (see Figure 11), or (2) the instability may be caused indirectly by the shift in the velocity of the core electrons required to maintain zero net current, similar to the heat flux mechanism. Of these two possibilities, the second mechanism is believed to be dominant. For the first mechanism rough

estimates show that the peak in the proton distribution function due to the upstreaming protons is simply too small to be unstable according to the Penrose criterion. Note that the contribution of the proton stream to F(V) is greatly reduced by the factor (m^-/m^+) in the combined one-dimensional distribution function, in addition to the fact that the distribution function for this stream is nearly six orders of magnitude below the peak due to the solar wind beam (see Figure 11). On the other hand, the proton flux associated with the upstreaming protons can be quite substantial, $\sim 5 \times 10^6$ protons $(cm^2\text{-sec})^{-1}$. The upstreaming protons must therefore cause a shift in the velocity of the core electrons with respect to the solar wind protons in order to maintain zero net current. If this shift is large enough to produce instability this mechanism would explain why the ion-acoustic waves driven by the upstreaming protons are so similar to the interplanetary ion-acoustic waves, since the mechanisms are essentially identical. Note that halo electrons streaming away from the sun and the sunward streaming protons both contribute in the same sense to the current imbalance. Detailed comparisons, however, often show that the intensities of the upstreaming protons are too small, by factors of 10 to 100, to produce velocity shifts exceeding the threshold for the ion-acoustic wave instability using a simple Maxwellian distribution for the core electrons. The detailed explanation of this discrepancy is not known, however one possibility is that the electron heat flux maintains the plasma near marginal stability for ion-acoustic waves, so that only a small current imbalance is needed to trigger the

instability. Also, Feldman et al. [1973b] have shown that protons streaming into the solar wind from the earth's bow shock produce substantial perturbations in the ambient solar wind electron distribution. These perturbations and their effect on the instability condition given by the Penrose criterion must be studied in greater detail before the generation mechanism of the upstream ion-acoustic waves can be completely resolved.

Numerous investigators have suggested possible roles which ion-acoustic turbulence may play in determining the large scale properties of the solar wind. It has been suggested that ion-acoustic waves can heat the solar wind ions [Fredricks, 1969], regulate the electron heat flux in the solar wind [Forslund, 1970; Schulz and Eviatar, 1972; Gary et al., 1976], and thermally couple the electron and ion distributions [Perkins, 1973]. The extent to which the ion-acoustic waves detected by Helios and IMP 6 and 8 play any significant role in these processes remains to be determined. At 1 A.U. the maximum intensities of the ion-acoustic turbulence are relatively small, with energy density ratios of only $\epsilon_o E^2/2nkT \simeq 10^{-5}$. The turbulence is, however, present a large fraction of the time and increases rapidly in intensity with decreasing radial distance from the sun. These factors all suggest that the presence of these waves must be given serious consideration in the overall understanding of the solar wind, particularly in relation to the regulation of the solar wind heat flux.

ACKNOWLEDGMENTS

The authors express their thanks to Dr. William Feldman from the Los Alamos Scientific Laboratory for providing the IMP-8 plasma density and temperature measurements used in this report.

The research at the University of Iowa was supported in part by NASA under Contracts NAS5-11279, NAS5-11431 and NAS5-11064, and Grants NGL-16-001-002 and NGL-16-001-043 and by the Office of Naval Research under Grant N00014-76-C-0016.

REFERENCES

Buneman, O., Instability, turbulence and conductivity in a current-carrying plasma, Phys. Rev. Lett., 1, 8, 1958.

Feldman, W. C., J. R. Asbridge, S. J. Bame, and M. D. Montgomery, Double ion streams in the solar wind, J. Geophys. Res., 78, 2017, 1973a.

Feldman, W. C., J. R. Asbridge, S. J. Bame, and M. D. Montgomery, Solar wind heat transport in the vicinity of the earth's bow shock, J. Geophys. Res., 78, 3697, 1973b.

Feldman, W. C., M. D. Montgomery, J. R. Asbridge, S. J. Bame, and H. R. Lewis, Interplanetary heat conduction - IMP 7 results, Solar Wind Three, Inst. of Geophys. and Planet. Physics, UCLA, Los Angeles, Calif., 334, 1974.

Feldman, W. C., J. R. Asbridge, S. J. Bame, M. D. Montgomery, and S. P. Gary, Solar wind electrons, J. Geophys. Res., 80, 4181, 1975.

Forslund, D. W., Instabilities associated with heat conduction in the solar wind and their consequences, J. Geophys. Res., 75, 17, 1970.

Frank, L. A., K. L. Ackerson, and R. P. Lepping, On hot tenuous plasmas, fireballs, and boundary layers in the earth's magnetotail, J. Geophys. Res., 34, 5859, 1976.

Fredricks, R. W., Electrostatic heating of solar wind ions beyond 0.1 A.U., J. Geophys. Res., 74, 2919, 1969.

Gary, S. P., W. C. Feldman, D. W. Forslund, and M. D. Montgomery, Heat flux instabilities in the solar wind, J. Geophys. Res., 81, 4197, 1975.

Gurnett, D. A., The earth as a radio source: terrestrial kilometric radiation, J. Geophys. Res., 79, 4227, 1974.

Gurnett, D. A. and L. A. Frank, The relationship of electron plasma oscillations to type III radio emission and low-energy solar electrons, Solar Physics, 45, 477, 1975.

Gurnett, D. A. and R. R. Anderson, Electron plasma oscillations associated with type III radio bursts, Science, 194, 1159, 1976.

Gurnett, D. A. and R. R. Anderson, Plasma wave electric fields in the solar wind: Initial results from Helios-1, J. Geophys. Res., 82, 632, 1977.

Krall, N. A. and A. W. Trivelpiece, Principles of Plasma Physics, McGraw-Hill, New York, 482, 1973.

Penrose, O., Electrostatic instability of a uniform non-Maxwellian plasma, Phys. Fluids, 3, 258, 1960.

Perkins, F., Heat conduction, plasma instabilities, and radio star scintillations in the solar wind, Astrophys. J., 179, 637, 1973.

Scarf, F. L., R. W. Fredricks, L. A. Frank, C. T. Russell, P. J. Coleman, Jr., and M. Neugebauer, Direct correlations of large amplitude waves with suprathermal protons in the upstream solar wind, J. Geophys. Res., 75, 7316, 1970.

Schulz, M. and A. Eviatar, Electron-temperature asymmetry and the structure of the solar wind, Cosmic Electrodynamics, 2, 402, 1972.

Stix, T. H., The Theory of Plasma Waves, McGraw-Hill, New York, 215, 1962.

Stringer, T. E., Electrostatic instabilities in current-carrying and counterstreaming plasmas, Plasma Physics, J. Nucl. Energy, C6, 267, 1964.

FIGURE CAPTIONS

Figure 1 A typical example of the ion-acoustic waves detected by the Helios 2 spacecraft at about 0.45 A.U. The solid lines and the vertical bars (solid black areas) indicate the peak and average electric field strengths. The intense noise at low frequencies, $\leq$ 311 Hz, is caused by interference from the spacecraft solar array.

Figure 2 A typical spectrum of the ion-acoustic turbulence at a selected interval from Figure 1. Note the distinct peak in the spectrum from about $(2 - 10)f_p^+$, and the large ratio of the peak to the average electric field strength indicative of very impulsive temporal variations.

Figure 3 Very high time resolution measurements from Figure 1, showing the impulsive burst-like temporal structure of the ion-acoustic turbulence.

Figure 4 The angular distribution of the electric field intensity of the ion-acoustic turbulence, showing that the electric field of this noise is oriented approximately parallel to the solar wind magnetic field.

Figure 5 A compressed time scale plot showing the electric field intensities for one solar rotation. Each peak and average point represents a 36-minute interval. These data show that a low level of ion-acoustic wave turbulence, at amplitudes of 10 to 100 $\mu V\ m^{-1}$, is present in the solar wind a substantial fraction of the time.

Figure 6 A statistical survey of the 36-minute peak field strength measurements of the type shown in Figure 5 for a total of two complete orbits around the sun. These data show that both the frequency and amplitude of the ion-acoustic wave turbulence increases systematically with decreasing radial distance from the sun, with $f_{max} \propto 1/R$.

Figure 7 A more detailed analysis of the broad-band electric field intensity as a function of the radial distance from the sun. The radial distance is plotted on a logarithmic scale, so that a power law dependence will be a straight line. The electric field amplitude varies approximately as 1/R.

Figure 8 An example of ion-acoustic waves detected upstream of the earth's magnetosphere in association with an intense burst of 1 to 10 keV protons streaming into the solar wind from the bow shock (see Plate 1).

Figure 9 A series of ion-acoustic wave events detected by IMP 8 for which no protons can be detected arriving from the bow shock (see Plate 2). These waves evidently correspond to the interplanetary ion-acoustic wave turbulence of the type detected by Helios far from the earth.

Figure 10 An intense burst of ion-acoustic waves detected during a period when a substantial anisotropy is evident in the low-energy electron distribution (see Plate 3).

Figure 11 The distribution function for the intense burst of protons observed streaming into the solar wind from the earth's bow shock from 0930 to 1030 UT in Plate 1. The $+V_x$ velocity axis is directed toward the sun. The dashed line gives the solar wind proton distribution function as determined from the Los Alamos plasma analyzer on IMP 8.

Figure 12 The angular distribution of the electric field intensity for an ion-acoustic wave event produced by upstreaming magnetosheath protons. These data show that the electric field of the proton-driven ion-acoustic waves is parallel to the solar wind magnetic field, essentially identical to the ion-acoustic waves detected by Helios far from the earth (compare with Figure 4).

Figure 13 The low-energy electron intensity variations associated with the burst of ion-acoustic waves shown in Figure 10. The dashed curve at $\varphi^{L}_{SE} = 124°$ gives the electron intensities perpendicular to the magnetic field and the solid curve at $\varphi^{L}_{SE} = 34°$ gives the intensities looking generally toward the sun and along the ecliptic plane projection of the magnetic field. The ion-acoustic waves occur during periods of substantial anisotropy in the low-energy electron intensities associated with the electron heat flux in the solar wind.

Figure 14 Further details of the anisotropic electron distribution associated with the burst of ion-acoustic waves shown in Figure 10, selected for times when the magnetic field is aligned parallel to the viewing direction of the LEPEDEA. At 1252 UT the anisotropy is very small and no ion-acoustic waves are present. At 1720 UT the anisotropy is large, particularly at the lower velocities, and the ion-acoustic wave intensities are correspondingly large.

Figure 15 A burst of ion-acoustic wave activity detected by IMP 6 in association with a density compression preceding a high-speed solar wind stream.

Figure 16 A comparison of the electric field amplitudes for the burst of ion-acoustic waves in Figure 15 using antennas of two different lengths. The deviation of the E_y/E_x ratio below one indicates that the wavelength of the waves are shorter than the longest antenna, L_y = 92.5 meters, at frequencies above about 3 kHz. The scale at the top of the illustration indicates the wavelength which would occur if the observed frequencies are entirely due to doppler shifts. Note the close correspondence of the upper frequency cutoff to the minimum wavelength $2\pi \lambda_D$ caused by Landau damping.

Figure 17 A comparison of the E_y/E_x ratio for a broadband plasmaspheric hiss emission observed a few hours after the event in Figure 16. Plasmaspheric hiss has wavelengths much longer than the antenna length. The close correspondence of the E_y/E_x ratio to one confirms the overall accuracy of this technique for detecting short wavelength effects.

Figure 18 An illustration showing the velocity shift, V_d, between the low-energy electrons and the solar wind protons, required to maintain zero net current when a substantial electron heat flux is present. If the velocity shift is sufficiently large the resulting double peak in the combined electron and proton distribution function, F(V), can cause the ion-acoustic mode to become unstable.

Plate 1 The LEPEDEA data corresponding to the electric field measurements in Figure 8, showing the occurrence of an intense burst of protons streaming towards the sun in direct correspondence with the burst of ion-acoustic waves from about 0920 to 1115 UT. These protons propagate from the earth's bow shock.

Plate 2 The LEPEDEA data corresponding to the electric field measurements in Figure 9, showing a series of ion-acoustic wave bursts for which no significant enhancement in either the electron or proton intensities can be identified in association with the ion-acoustic wave activity.

Plate 3 The LEPEDEA data corresponding to the electric field measurements in Figure 10, showing an event in which the ion-acoustic turbulence (from about 1540 to 1930 UT) is closely correlated with the occurrence of a greatly enhanced anisotropy in the low-energy solar wind electron distribution. This anisotropy is clearly evident in the electron sector spectrogram from about 1540 to 1900 UT.

Note: Plates 1, 2 and 3 will be published in color.

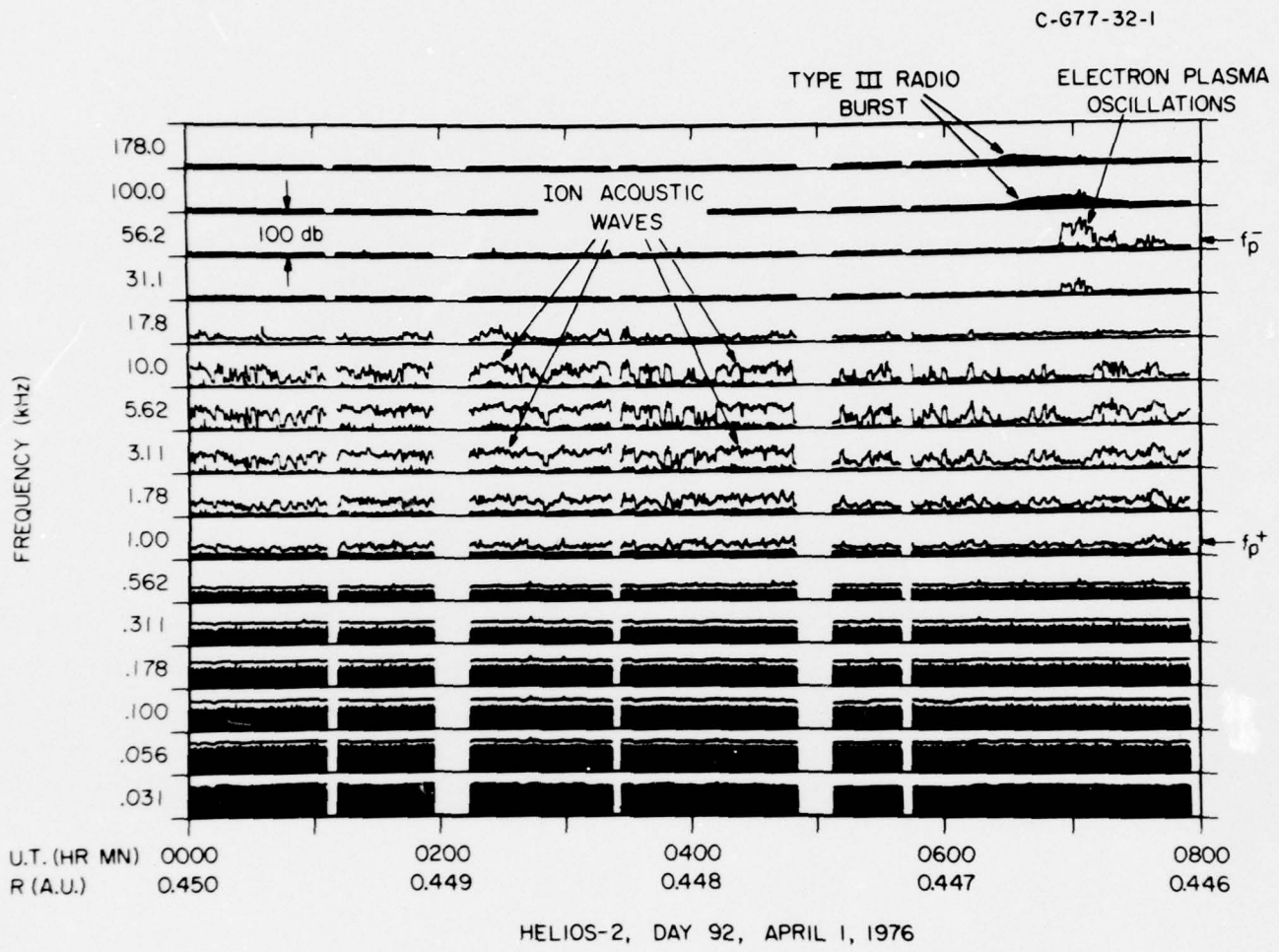
C-G77-32-1
TYPE III RADIO BURST
ELECTRON PLASMA OSCILLATIONS
ION ACOUSTIC WAVES
100 db
f_p^-
f_p^+
FREQUENCY (kHz)
178.0
100.0
56.2
31.1
17.8
10.0
5.62
3.11
1.78
1.00
.562
.311
.178
.100
.056
.031
U.T. (HR MN) 0000 0200 0400 0600 0800
R (A.U.) 0.450 0.449 0.448 0.447 0.446
HELIOS-2, DAY 92, APRIL 1, 1976

Figure 1

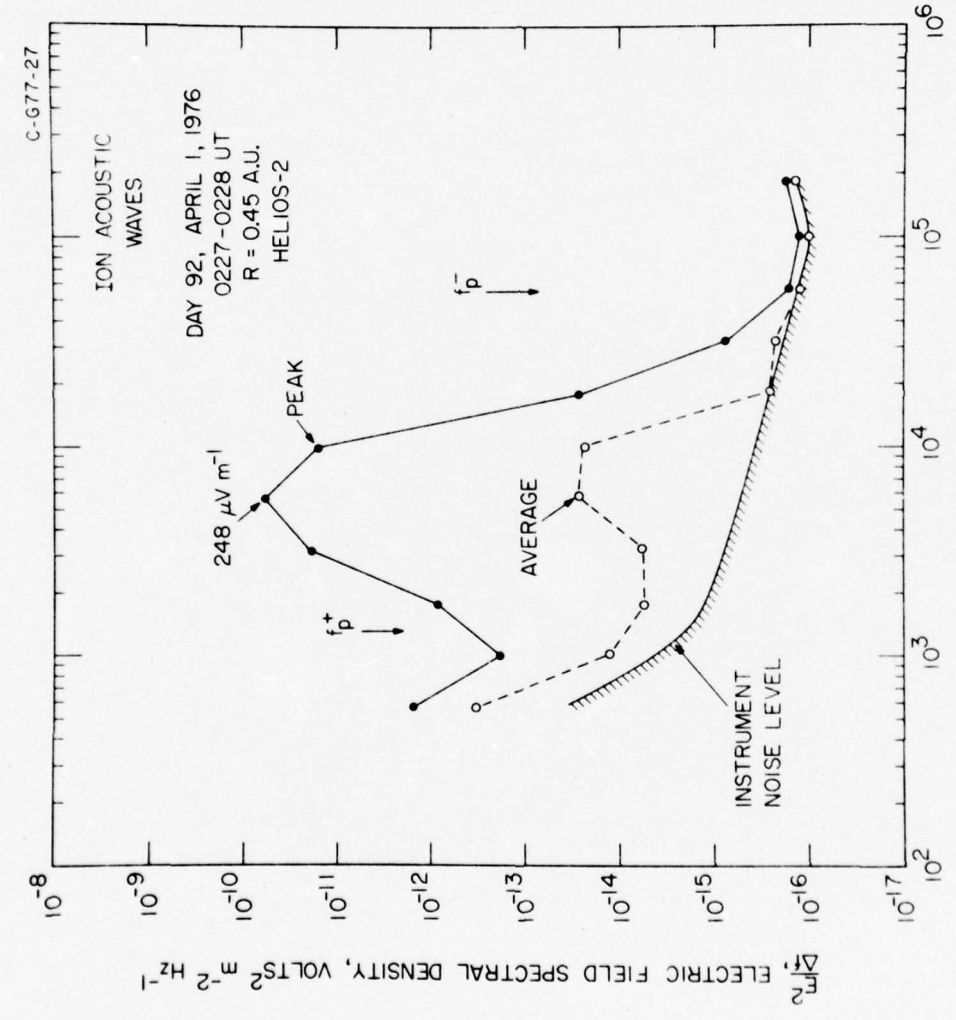
C-G77-27
ION ACOUSTIC WAVES
DAY 92, APRIL 1, 1976
0227-0228 UT
R = 0.45 A.U.
HELIOS-2
248 μV m⁻¹
PEAK
AVERAGE
INSTRUMENT NOISE LEVEL
FREQUENCY, Hz
ELECTRIC FIELD SPECTRAL DENSITY, VOLTS² m⁻² Hz⁻¹

Figure 2

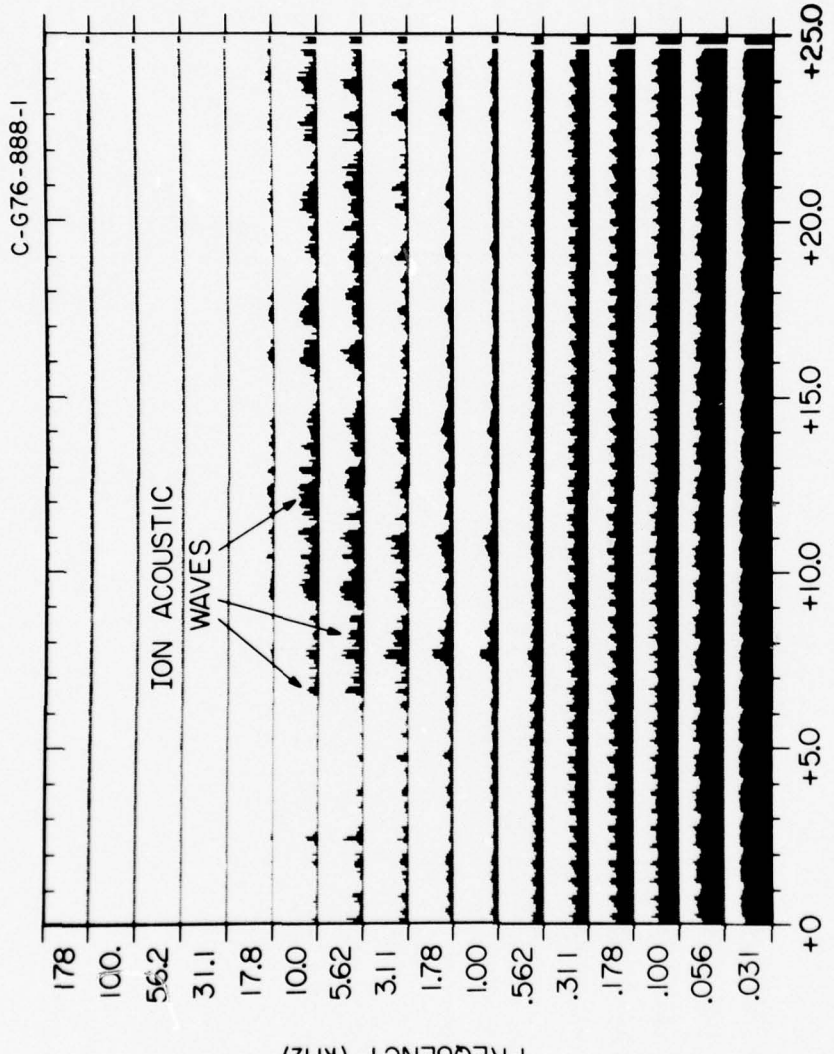
C-G76-888-1
ION ACOUSTIC
WAVES
178
100.
56.2
31.1
17.8
10.0
5.62
3.11
1.78
1.00
.562
.311
.178
.100
.056
.031
FREQUENCY (kHz)
+0
+5.0
+10.0
+15.0
+20.0
+25.0
TIME (SEC)
HELIOS-2, DAY 92, APRIL 1, 1976
START TIME 0257:25.70 U.T., R = 0.45 A.U.

Figure 3

A-G76-167-3

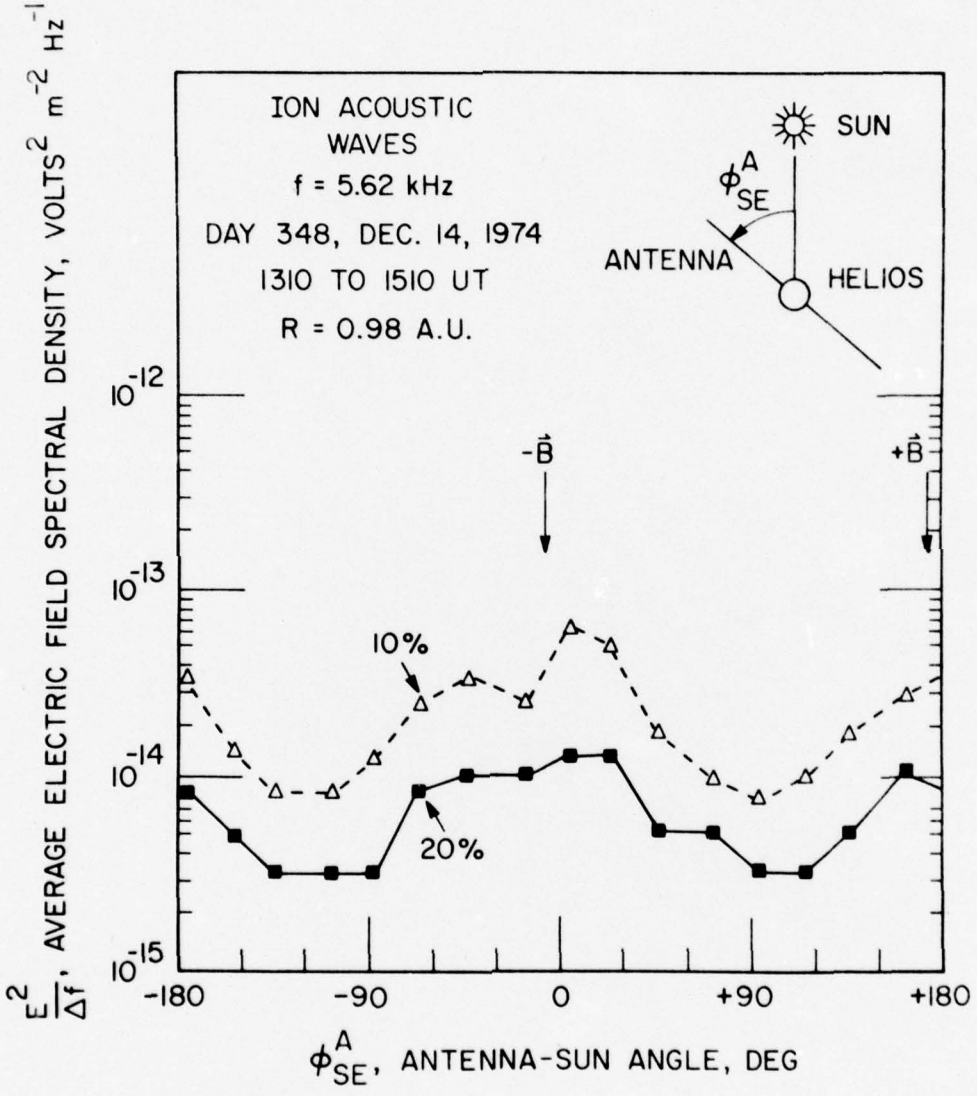

Figure 4

C-G77-43

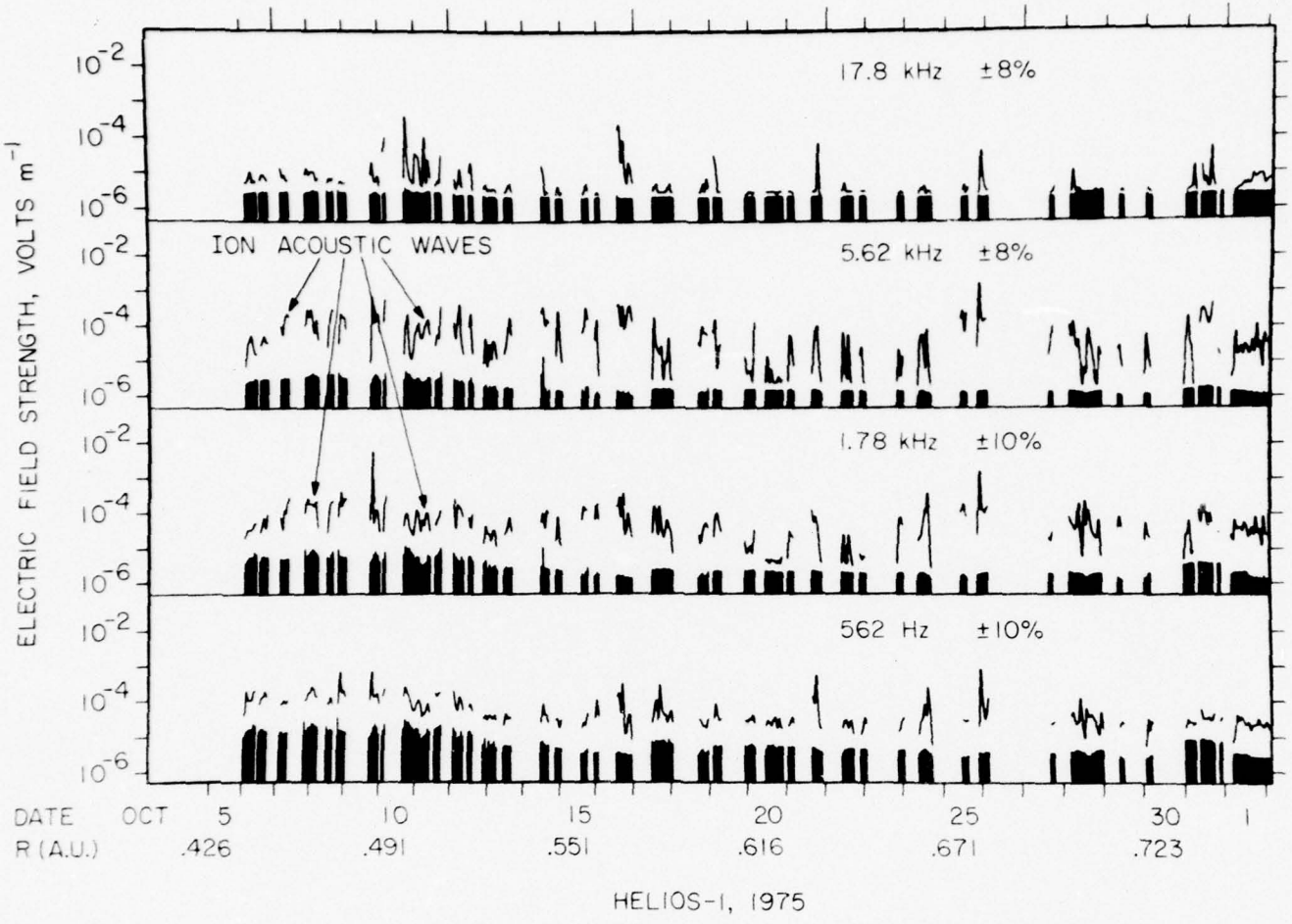

HELIOS-1, 1975

Figure 5

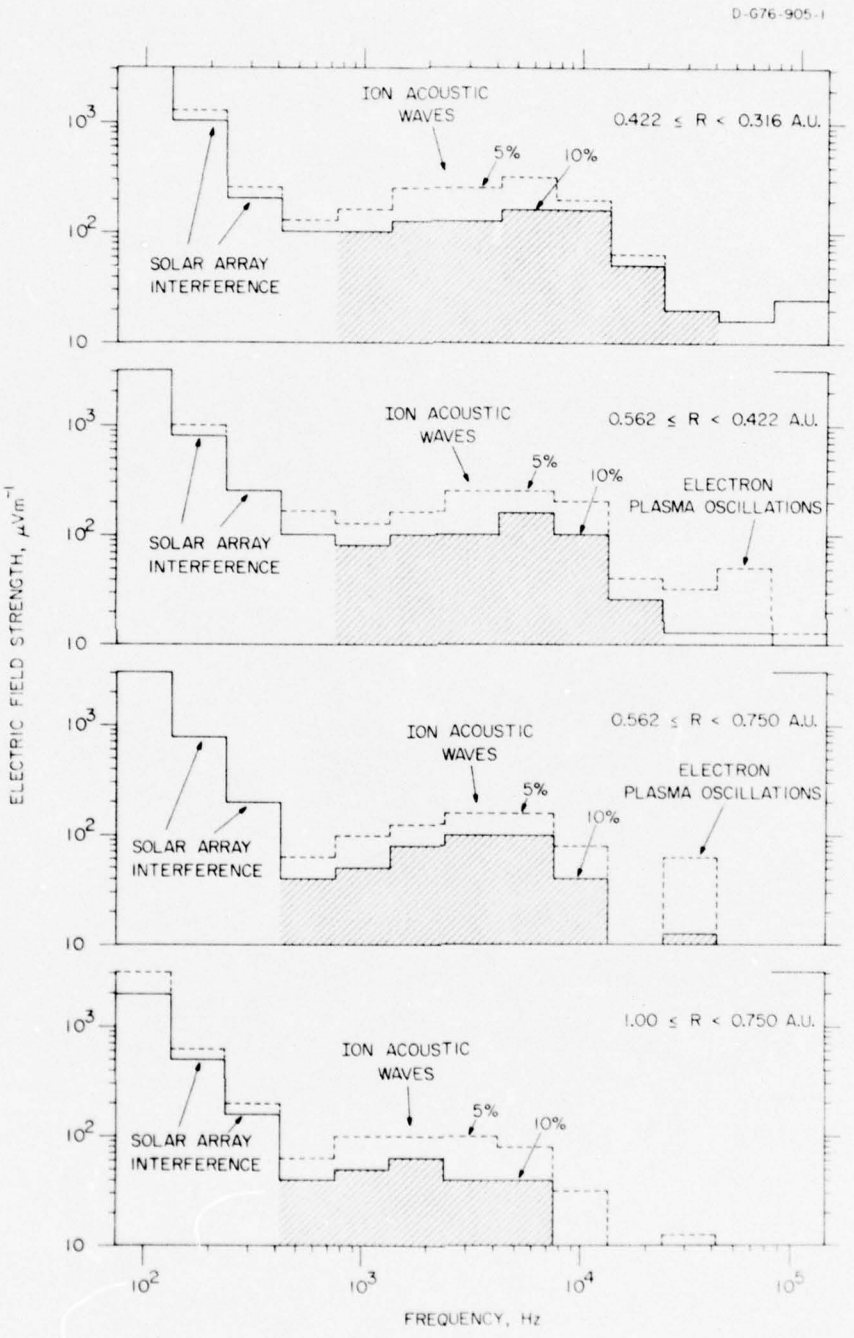
D-G76-905-1
ELECTRIC FIELD STRENGTH, μVm⁻¹
FREQUENCY, Hz
ION ACOUSTIC WAVES
SOLAR ARRAY INTERFERENCE
5%
10%
0.422 ≤ R < 0.316 A.U.
0.562 ≤ R < 0.422 A.U.
ELECTRON PLASMA OSCILLATIONS
0.562 ≤ R < 0.750 A.U.
1.00 ≤ R < 0.750 A.U.

Figure 6

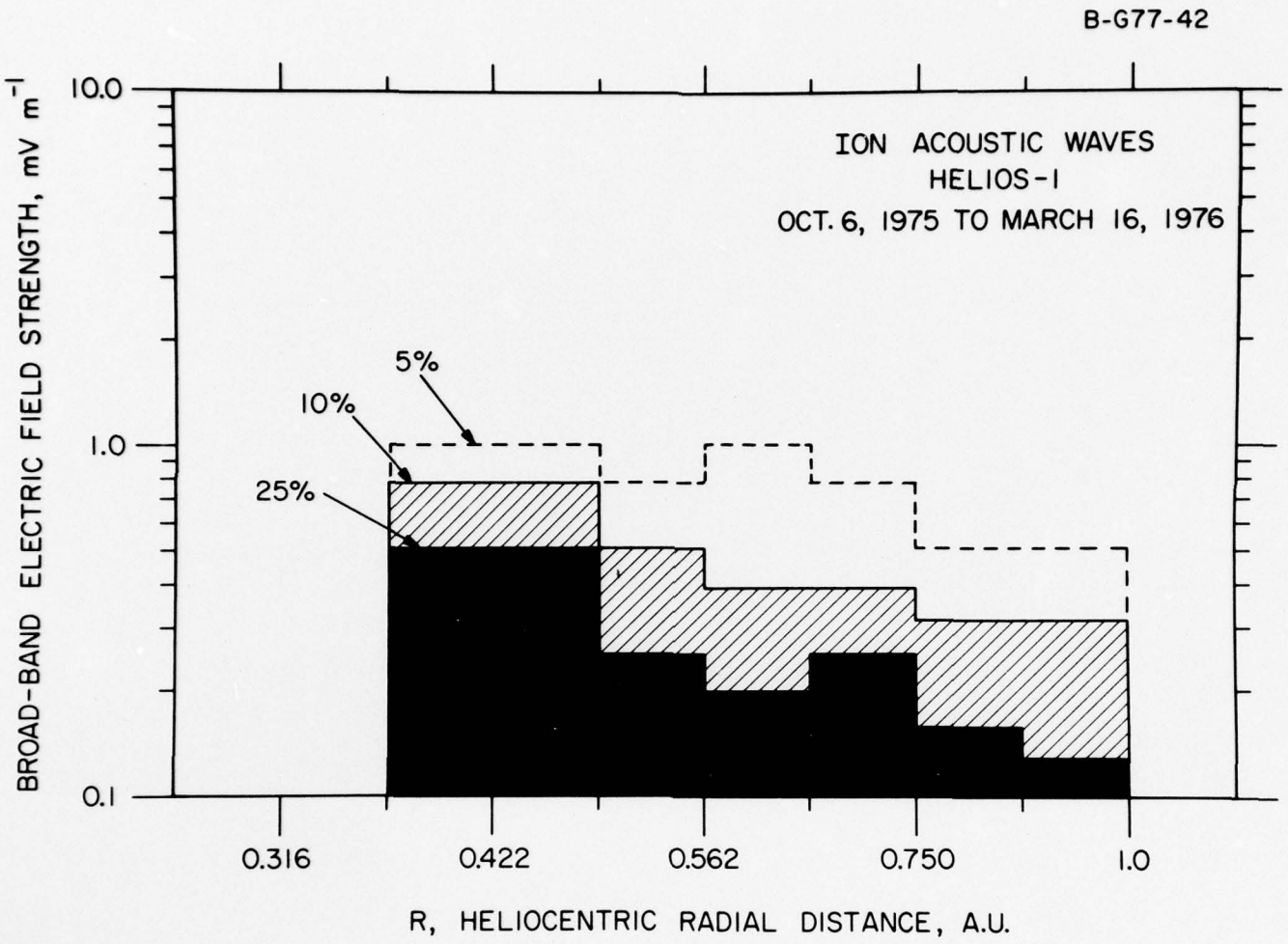
B-G77-42
ION ACOUSTIC WAVES
HELIOS-1
OCT. 6, 1975 TO MARCH 16, 1976
BROAD-BAND ELECTRIC FIELD STRENGTH, mV m^{-1}
10.0
1.0
0.1
5%
10%
25%
0.316
0.422
0.562
0.750
1.0
R, HELIOCENTRIC RADIAL DISTANCE, A.U.

Figure 7

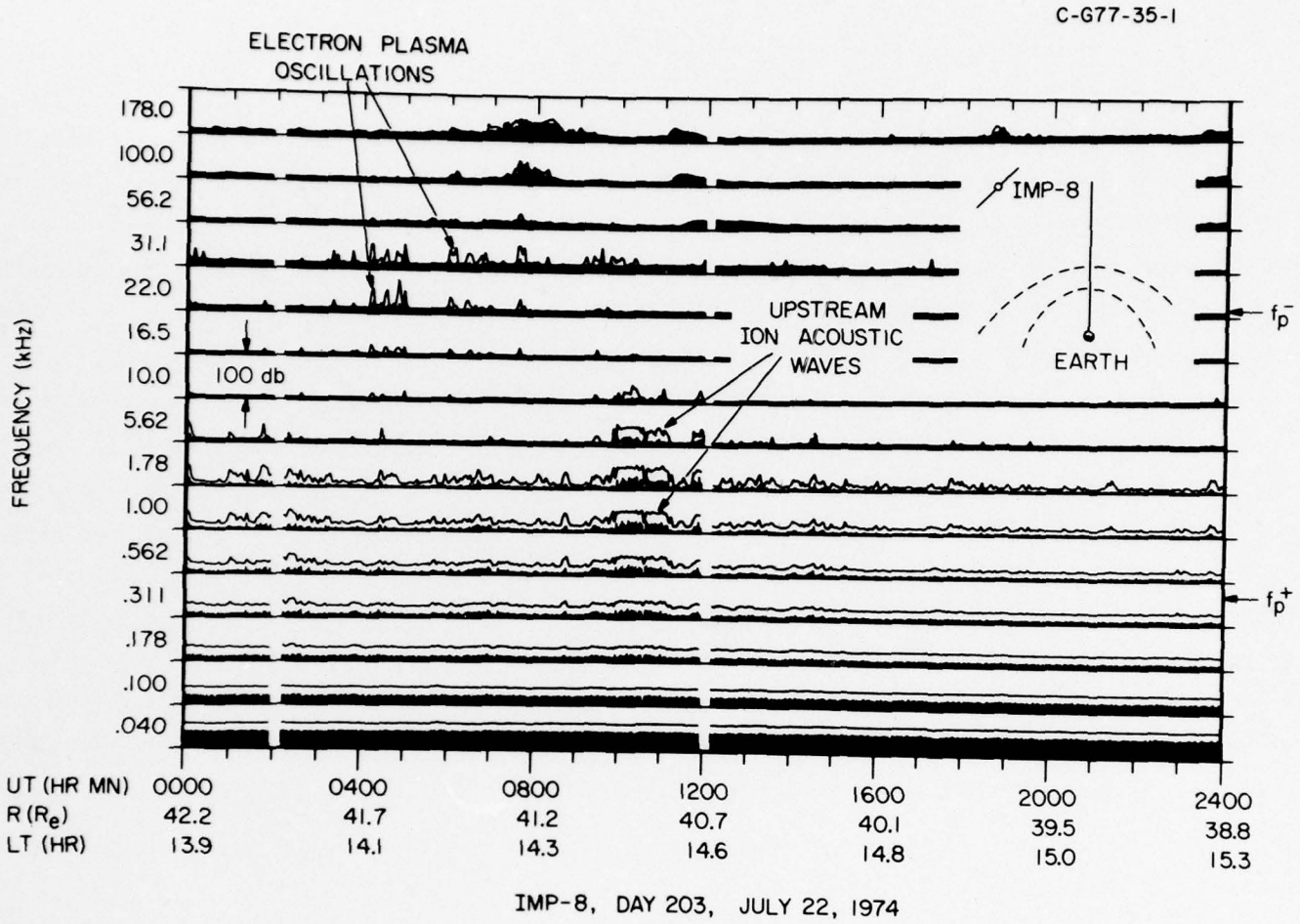
C-G77-35-1
ELECTRON PLASMA OSCILLATIONS
178.0
100.0
56.2
31.1
22.0
16.5
10.0
5.62
1.78
1.00
.562
.311
.178
.100
.040
FREQUENCY (kHz)
100 db
IMP-8
UPSTREAM ION ACOUSTIC WAVES
EARTH
f_p^-
f_p^+
UT (HR MN) 0000 0400 0800 1200 1600 2000 2400
R (R_e) 42.2 41.7 41.2 40.7 40.1 39.5 38.8
LT (HR) 13.9 14.1 14.3 14.6 14.8 15.0 15.3
IMP-8, DAY 203, JULY 22, 1974

Figure 8

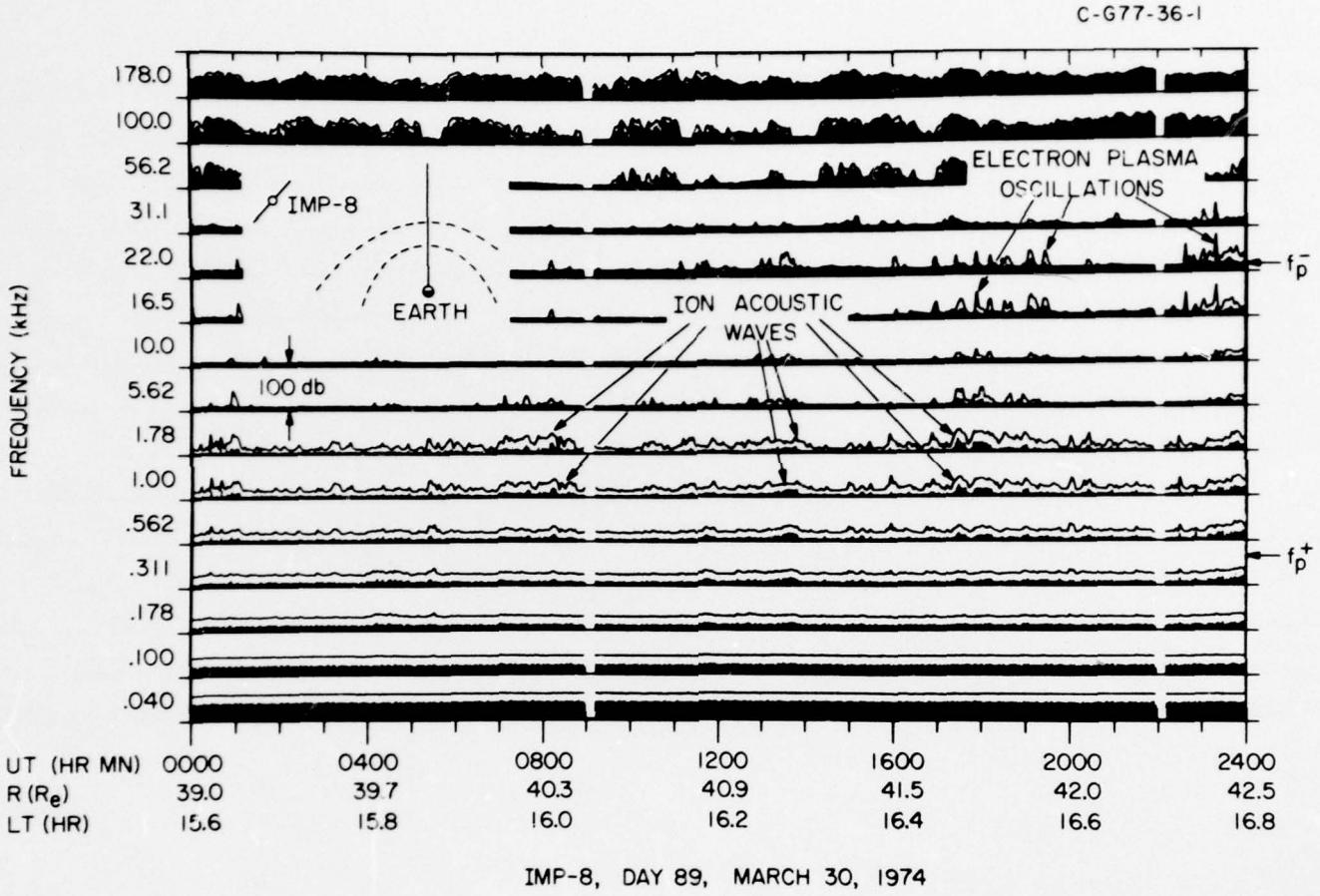
C-G77-36-1
178.0
100.0
56.2
31.1
22.0
16.5
10.0
5.62
1.78
1.00
.562
.311
.178
.100
.040
FREQUENCY (kHz)
IMP-8
EARTH
100 db
ELECTRON PLASMA
OSCILLATIONS
ION ACOUSTIC
WAVES
f_p^-
f_p^+
UT (HR MN) 0000 0400 0800 1200 1600 2000 2400
R (R_e) 39.0 39.7 40.3 40.9 41.5 42.0 42.5
LT (HR) 15.6 15.8 16.0 16.2 16.4 16.6 16.8
IMP-8, DAY 89, MARCH 30, 1974

Figure 9

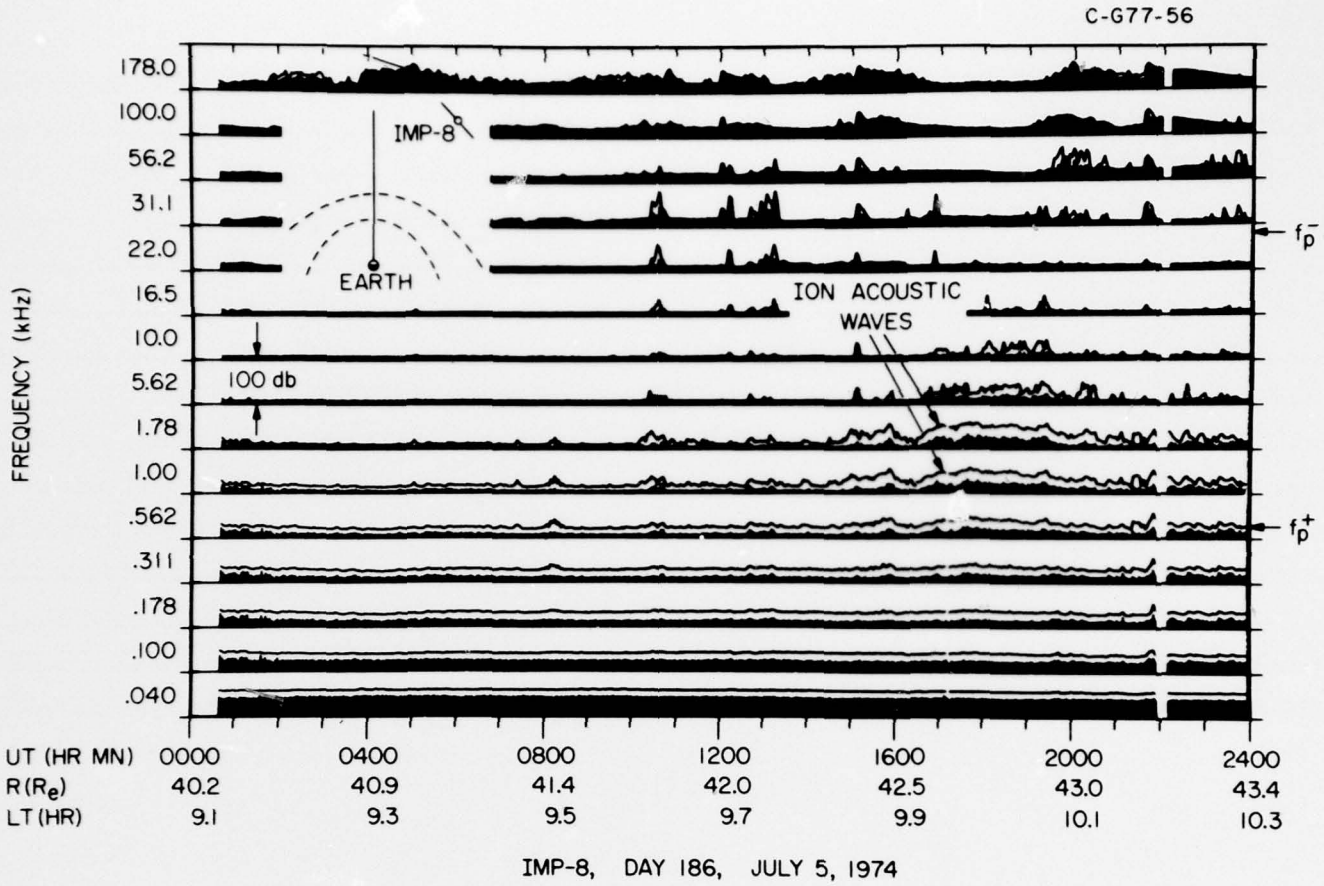
C-G77-56
178.0
100.0
56.2
31.1
22.0
16.5
10.0
5.62
1.78
1.00
.562
.311
.178
.100
.040
FREQUENCY (kHz)
IMP-8
EARTH
ION ACOUSTIC
WAVES
100 db
f_p^-
f_p^+
UT (HR MN) 0000 0400 0800 1200 1600 2000 2400
R(R_e) 40.2 40.9 41.4 42.0 42.5 43.0 43.4
LT (HR) 9.1 9.3 9.5 9.7 9.9 10.1 10.3
IMP-8, DAY 186, JULY 5, 1974

Figure 10

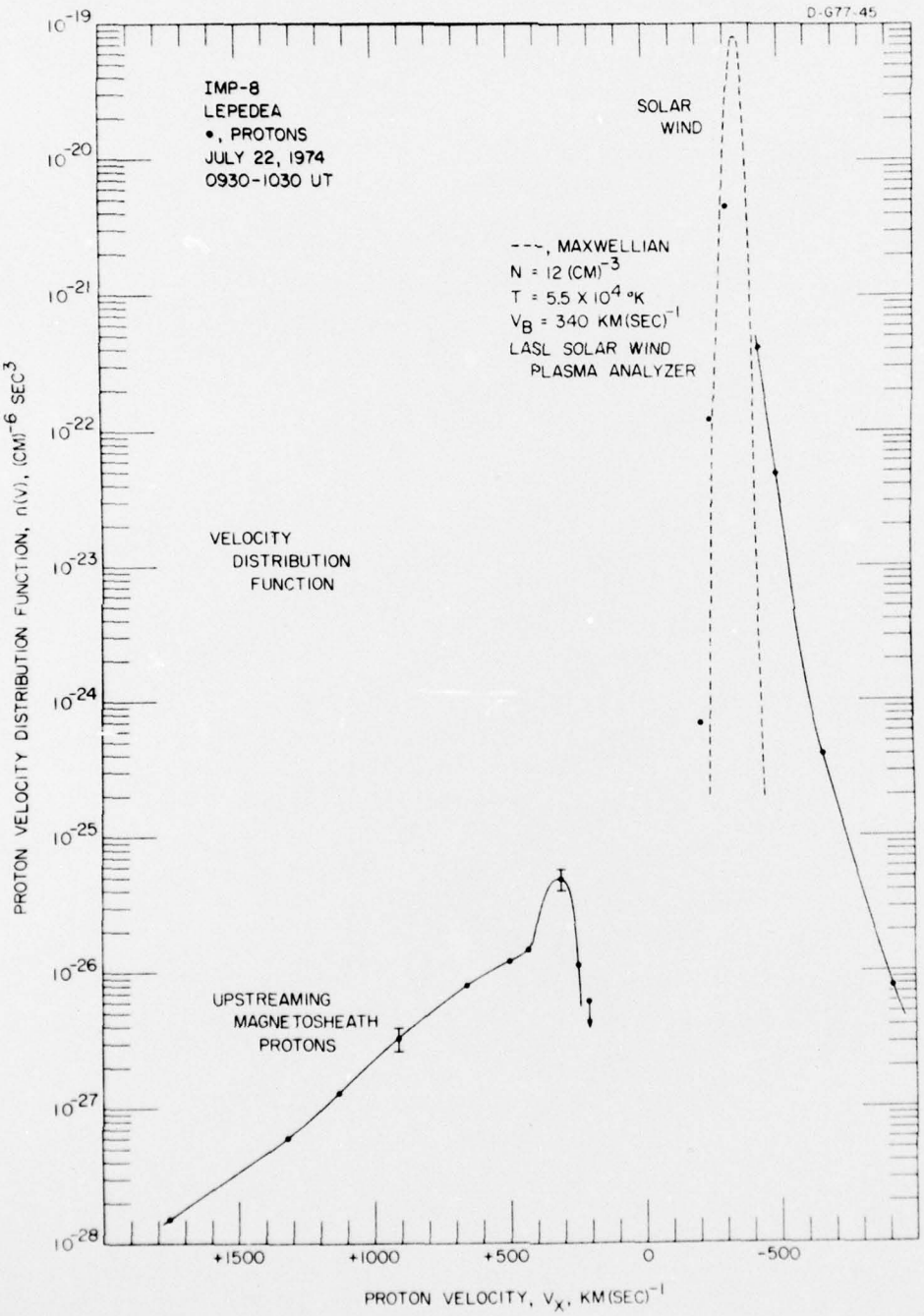
D-G77-45
IMP-8
LEPEDEA
•, PROTONS
JULY 22, 1974
0930-1030 UT
SOLAR WIND
---, MAXWELLIAN
N = 12 (CM)$^{-3}$
T = 5.5 X 10^4 °K
V_B = 340 KM(SEC)$^{-1}$
LASL SOLAR WIND PLASMA ANALYZER
VELOCITY DISTRIBUTION FUNCTION
UPSTREAMING MAGNETOSHEATH PROTONS
PROTON VELOCITY DISTRIBUTION FUNCTION, n(V), (CM)$^{-6}$ SEC^3
10^{-19}
10^{-20}
10^{-21}
10^{-22}
10^{-23}
10^{-24}
10^{-25}
10^{-26}
10^{-27}
10^{-28}
+1500
+1000
+500
0
-500
PROTON VELOCITY, V_X, KM(SEC)$^{-1}$

Figure 11

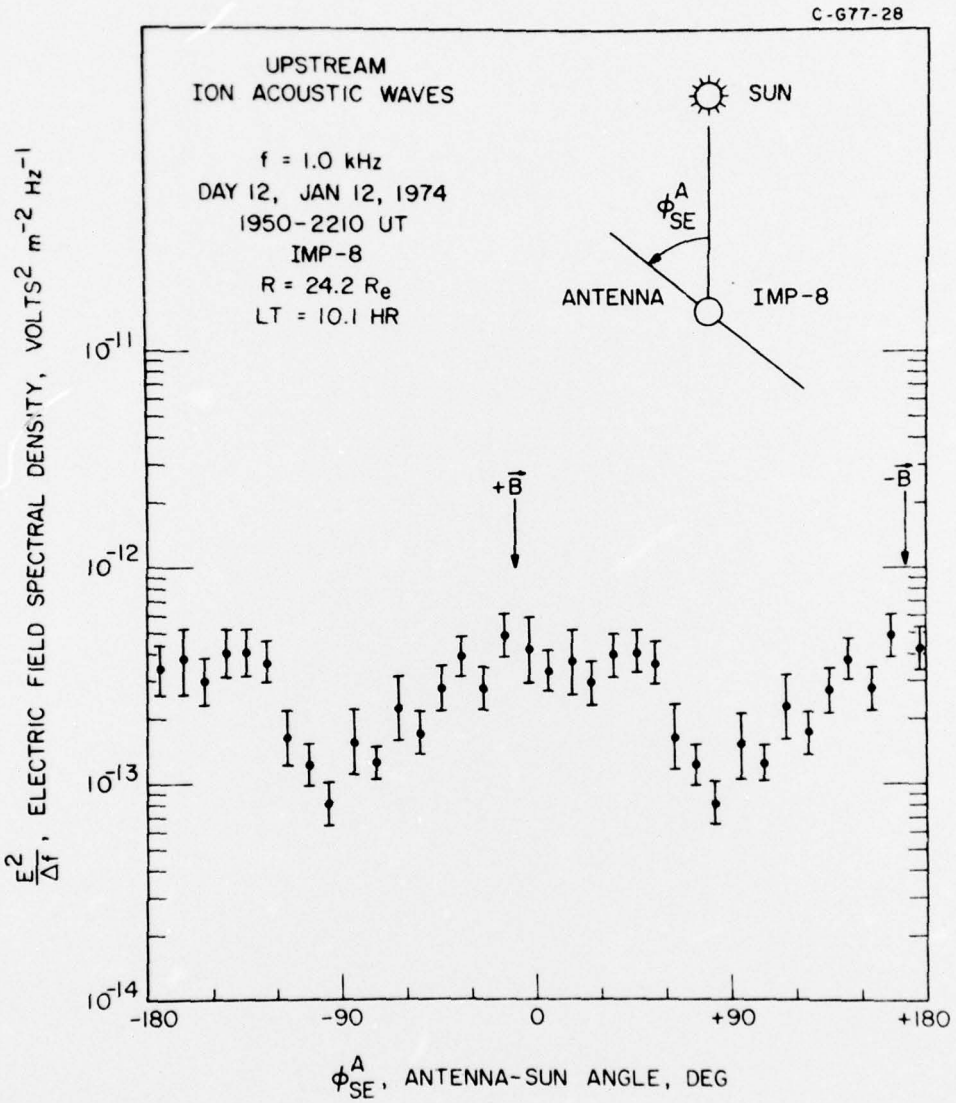
C-G77-28
UPSTREAM
ION ACOUSTIC WAVES
f = 1.0 kHz
DAY 12, JAN 12, 1974
1950-2210 UT
IMP-8
R = 24.2 Re
LT = 10.1 HR
SUN
ANTENNA
IMP-8
+B
-B
10^-11
10^-12
10^-13
10^-14
-180
-90
0
+90
+180
E^2/Δf, ELECTRIC FIELD SPECTRAL DENSITY, VOLTS^2 m^-2 Hz^-1
φ^A_SE, ANTENNA-SUN ANGLE, DEG

Figure 12

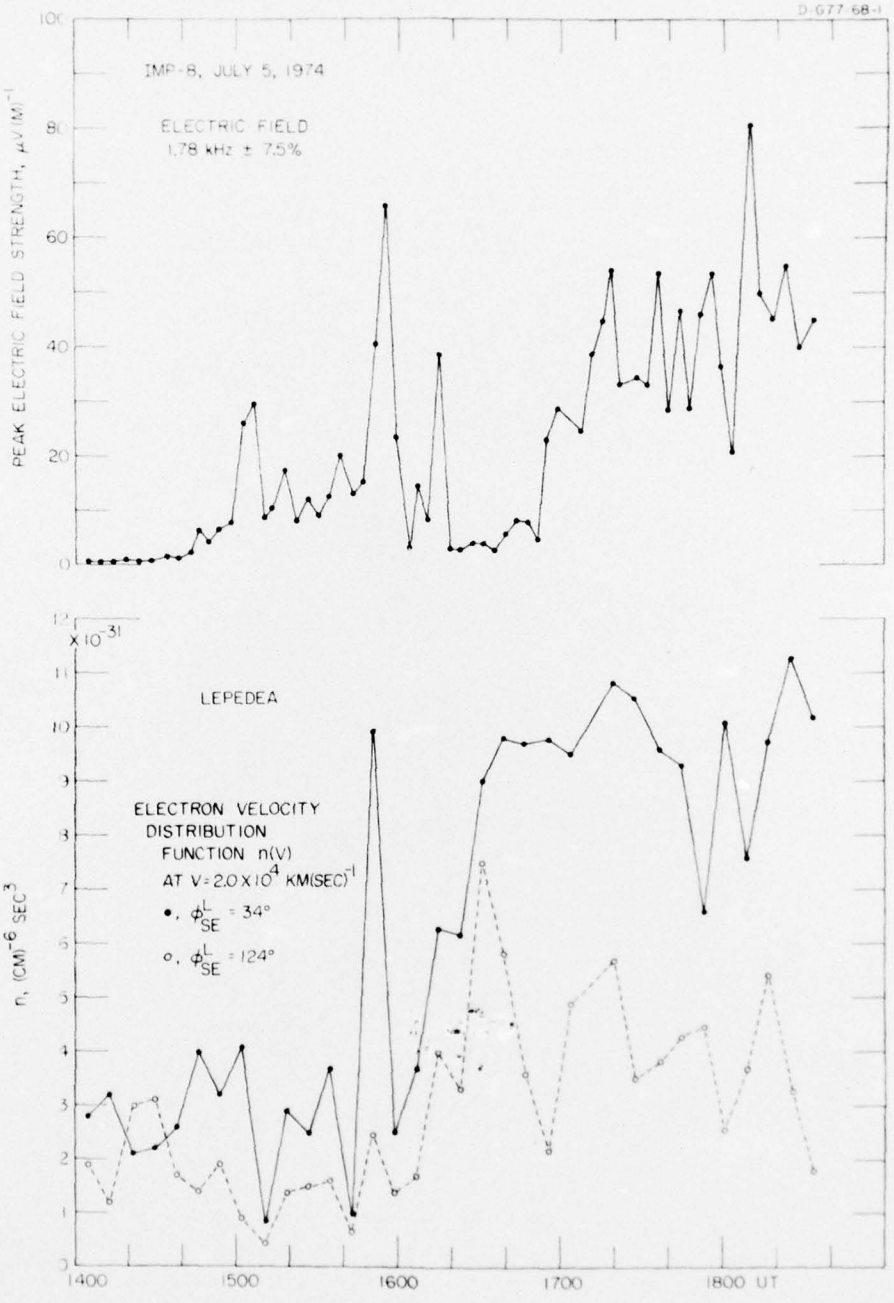
D-677-68-1
IMP-8, JULY 5, 1974
ELECTRIC FIELD
1.78 kHz ± 7.5%
PEAK ELECTRIC FIELD STRENGTH, μV/(M)^-1
100
80
60
40
20
0
X 10^-31
LEPEDEA
ELECTRON VELOCITY
DISTRIBUTION
FUNCTION n(V)
AT V = 2.0 X 10^4 KM(SEC)^-1
•, φ^L_SE = 34°
o, φ^L_SE = 124°
n, (CM)^-6 SEC^3
12
11
10
9
8
7
6
5
4
3
2
1
0
1400
1500
1600
1700
1800 UT

Figure 13

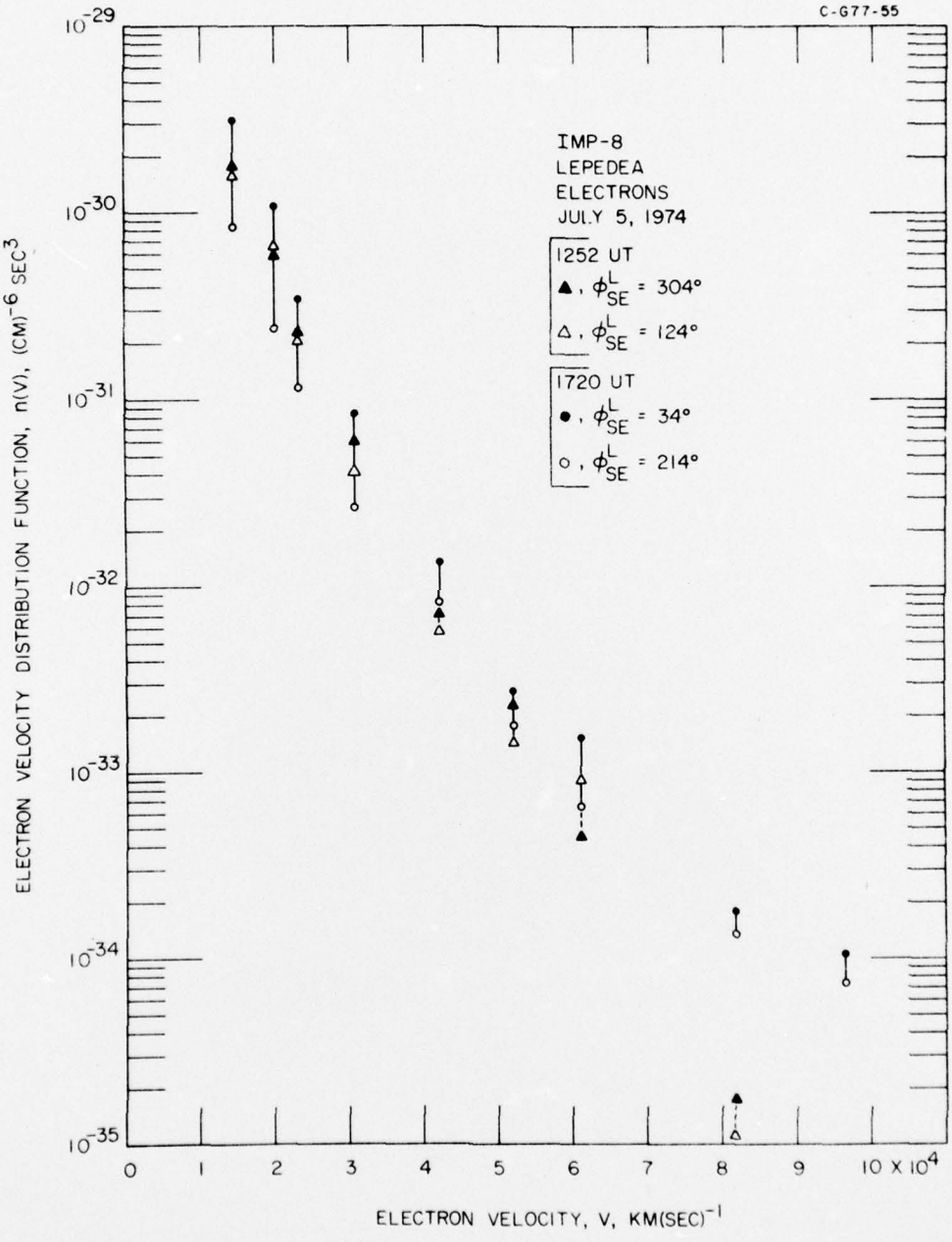
C-G77-55
IMP-8
LEPEDEA
ELECTRONS
JULY 5, 1974
1252 UT
▲, ϕ_{SE}^{L} = 304°
△, ϕ_{SE}^{L} = 124°
1720 UT
●, ϕ_{SE}^{L} = 34°
○, ϕ_{SE}^{L} = 214°
ELECTRON VELOCITY DISTRIBUTION FUNCTION, n(V), (CM)$^{-6}$ SEC^{3}
10^{-29}
10^{-30}
10^{-31}
10^{-32}
10^{-33}
10^{-34}
10^{-35}
0 1 2 3 4 5 6 7 8 9 10 X 10^{4}
ELECTRON VELOCITY, V, KM(SEC)$^{-1}$

Figure 14

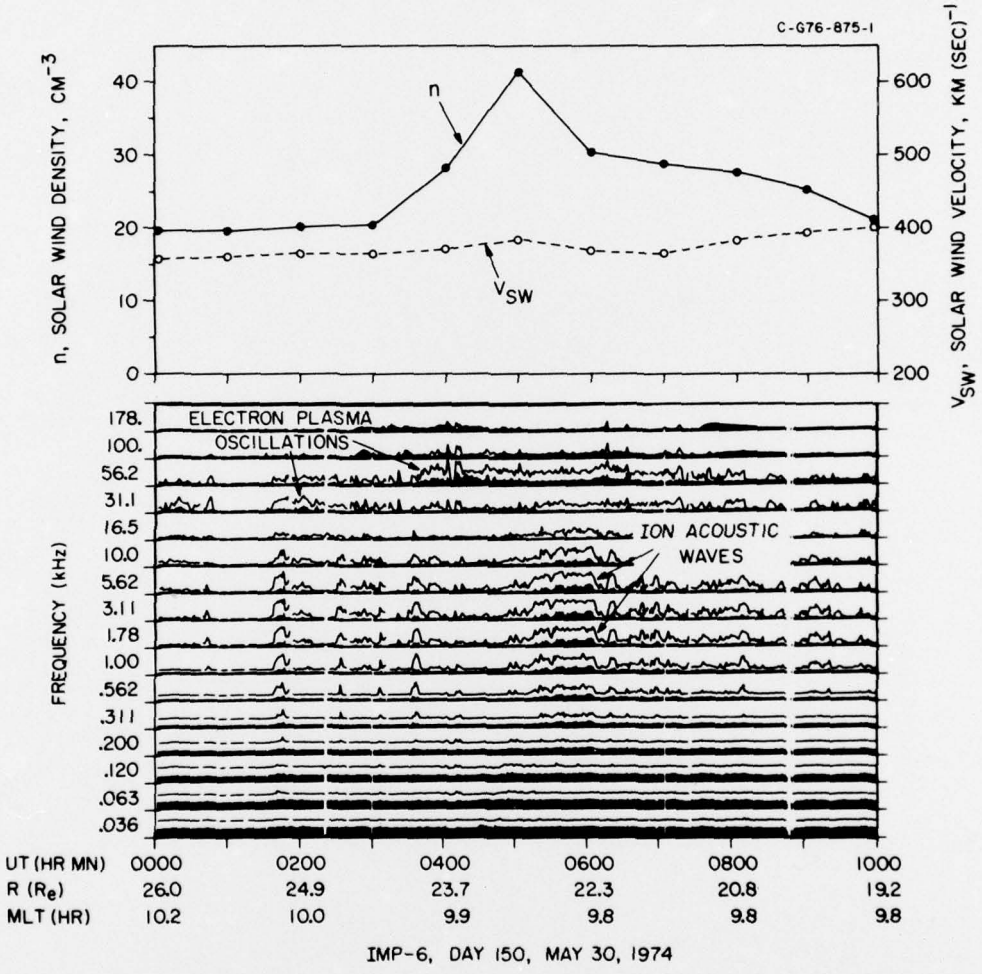
C-G76-875-1
n, SOLAR WIND DENSITY, CM^{-3}
V_{SW}, SOLAR WIND VELOCITY, KM (SEC)$^{-1}$
n
V_{SW}
40
30
20
10
0
600
500
400
300
200
FREQUENCY (kHz)
178.
100.
56.2
31.1
16.5
10.0
5.62
3.11
1.78
1.00
.562
.311
.200
.120
.063
.036
ELECTRON PLASMA
OSCILLATIONS
ION ACOUSTIC
WAVES
UT (HR MN) 0000 0200 0400 0600 0800 1000
R (R_e) 26.0 24.9 23.7 22.3 20.8 19.2
MLT (HR) 10.2 10.0 9.9 9.8 9.8 9.8
IMP-6, DAY 150, MAY 30, 1974

Figure 15

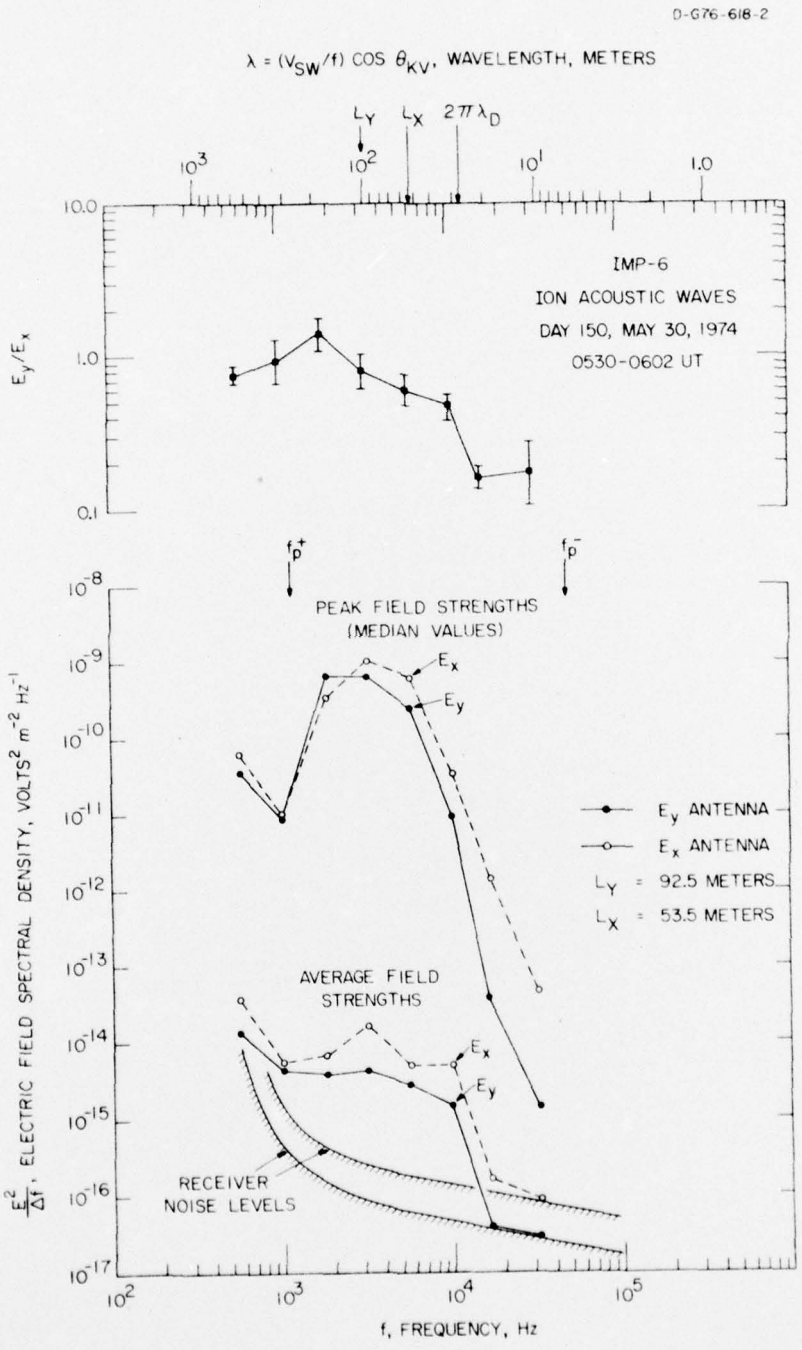
D-G76-618-2
λ = (V_SW/f) COS θ_KV, WAVELENGTH, METERS
L_Y
L_X
2πλ_D
10^3
10^2
10^1
1.0
10.0
1.0
0.1
E_y/E_x
IMP-6
ION ACOUSTIC WAVES
DAY 150, MAY 30, 1974
0530-0602 UT
f_p^+
f_p^-
PEAK FIELD STRENGTHS
(MEDIAN VALUES)
E_x
E_y
E_y ANTENNA
E_x ANTENNA
L_Y = 92.5 METERS
L_X = 53.5 METERS
AVERAGE FIELD
STRENGTHS
RECEIVER
NOISE LEVELS
E²/Δf, ELECTRIC FIELD SPECTRAL DENSITY, VOLTS² m⁻² Hz⁻¹
10^-8
10^-9
10^-10
10^-11
10^-12
10^-13
10^-14
10^-15
10^-16
10^-17
10^2
10^3
10^4
10^5
f, FREQUENCY, Hz

Figure 16

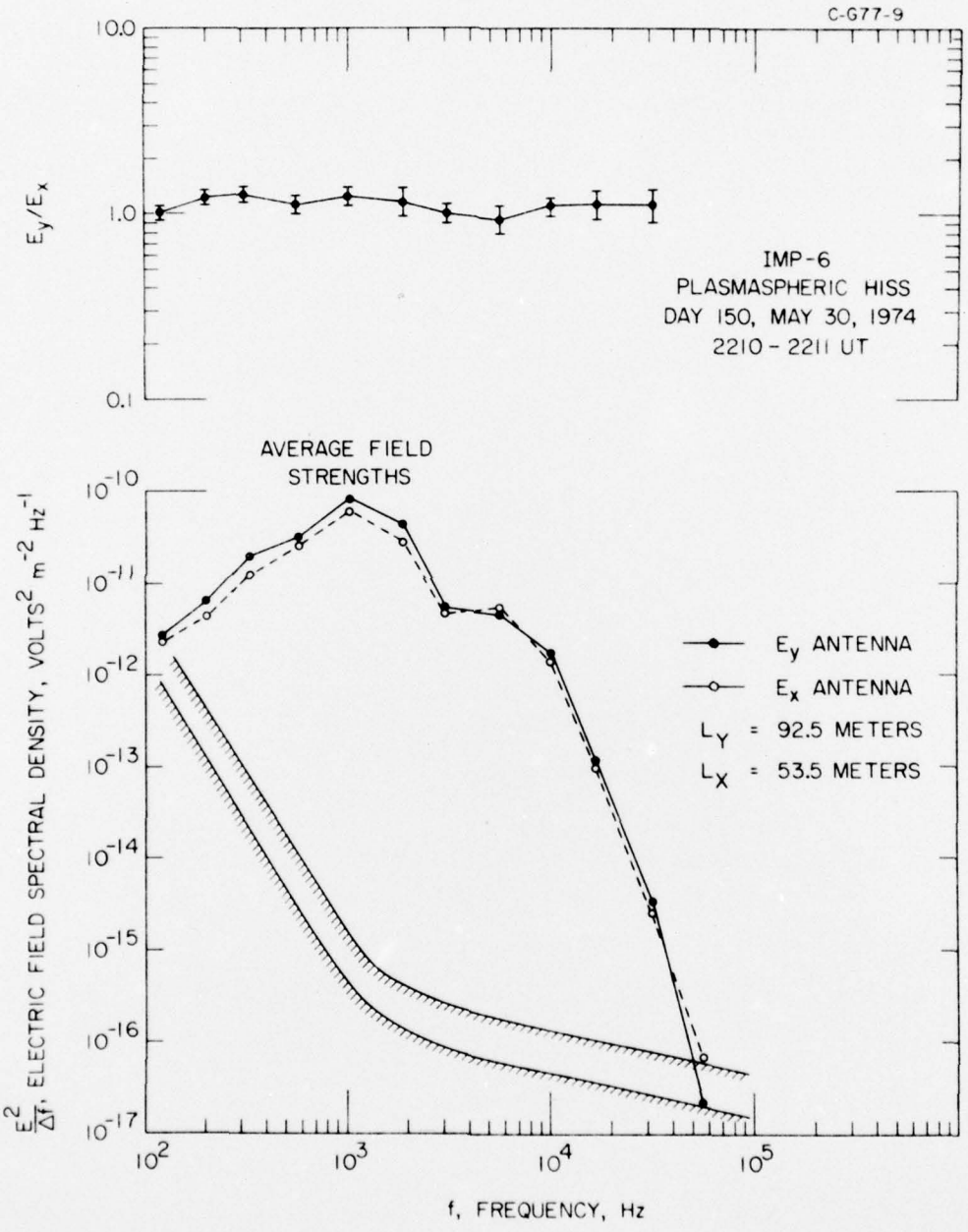
C-G77-9
10.0
1.0
0.1
E_y/E_x
IMP-6
PLASMASPHERIC HISS
DAY 150, MAY 30, 1974
2210 - 2211 UT
AVERAGE FIELD
STRENGTHS
10^{-10}
10^{-11}
10^{-12}
10^{-13}
10^{-14}
10^{-15}
10^{-16}
10^{-17}
$\frac{E^2}{\Delta f}$, ELECTRIC FIELD SPECTRAL DENSITY, VOLTS^2 m^{-2} Hz^{-1}
E_y ANTENNA
E_x ANTENNA
L_Y = 92.5 METERS
L_X = 53.5 METERS
10^2
10^3
10^4
10^5
f, FREQUENCY, Hz

Figure 17

B-G77-65

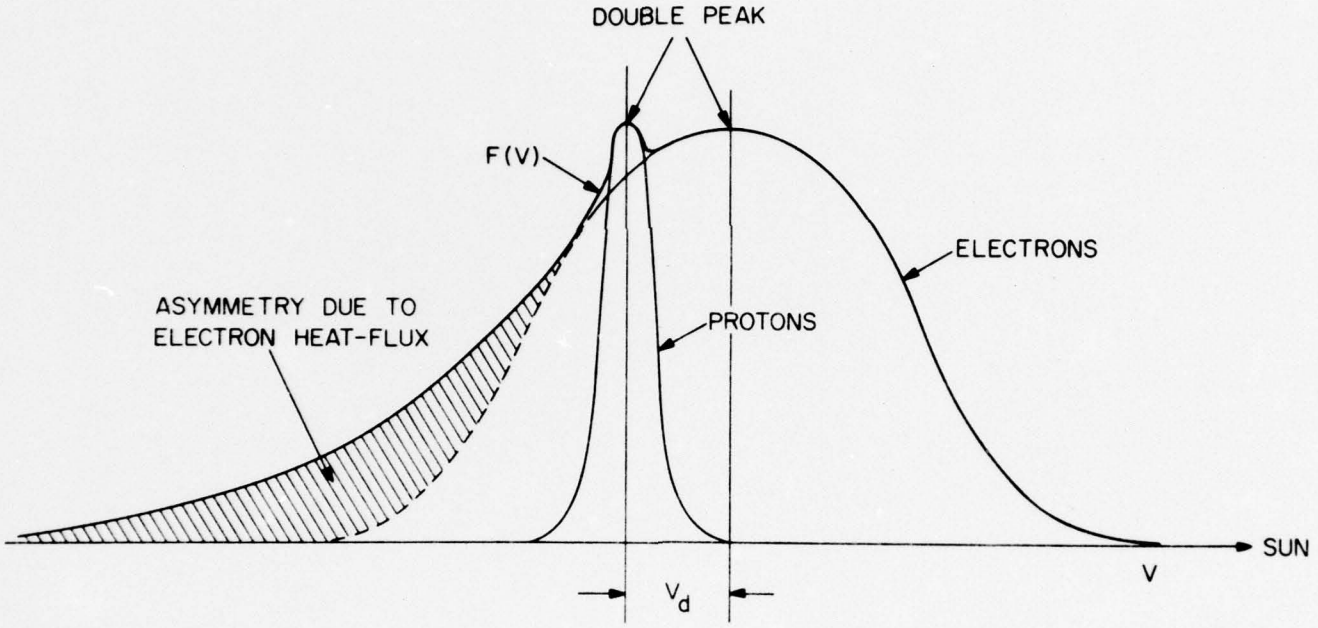

Figure 18

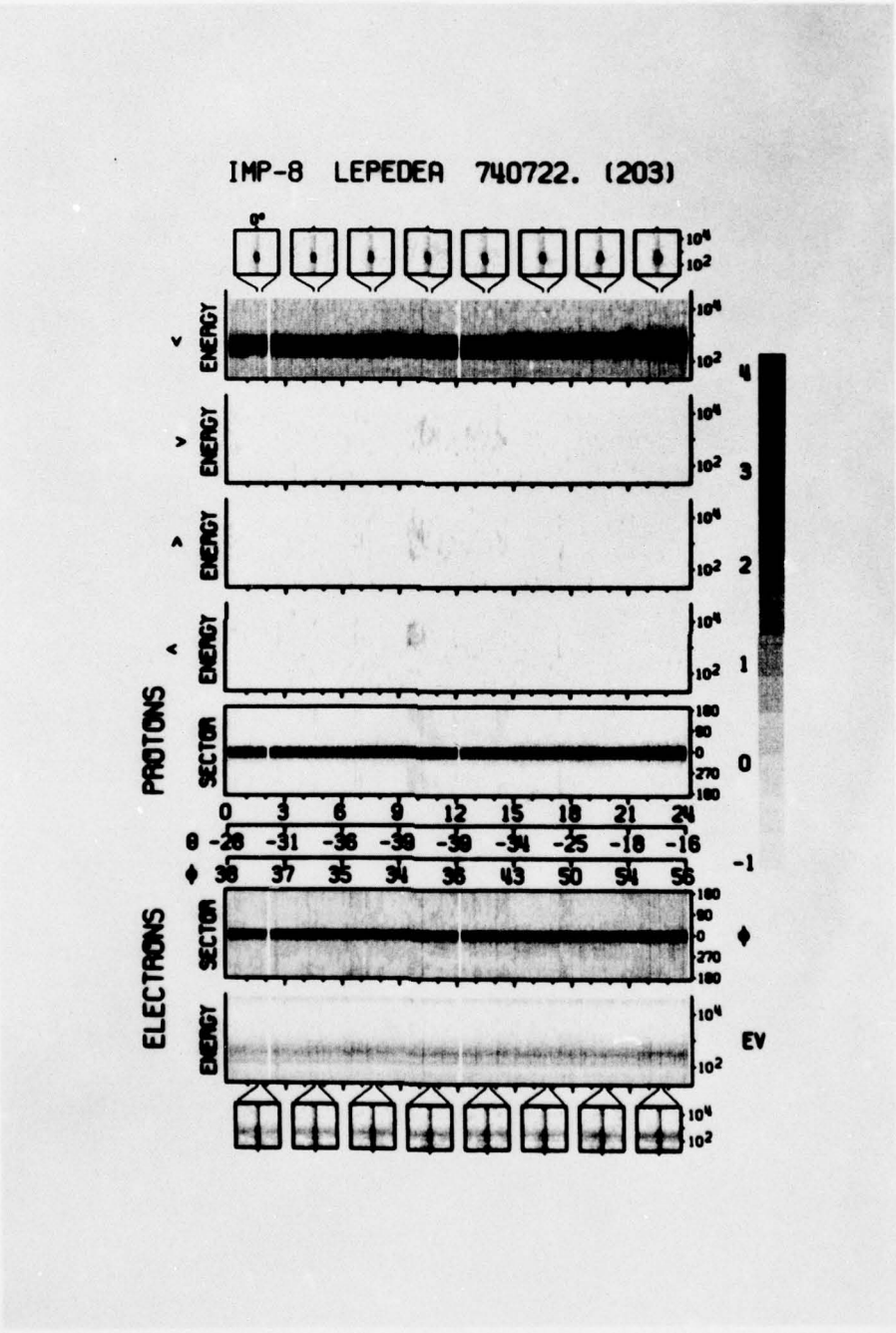
IMP-8 LEPEDEA 740722. (203)
PROTONS
ELECTRONS
ENERGY
SECTOR
EV

Plate 1

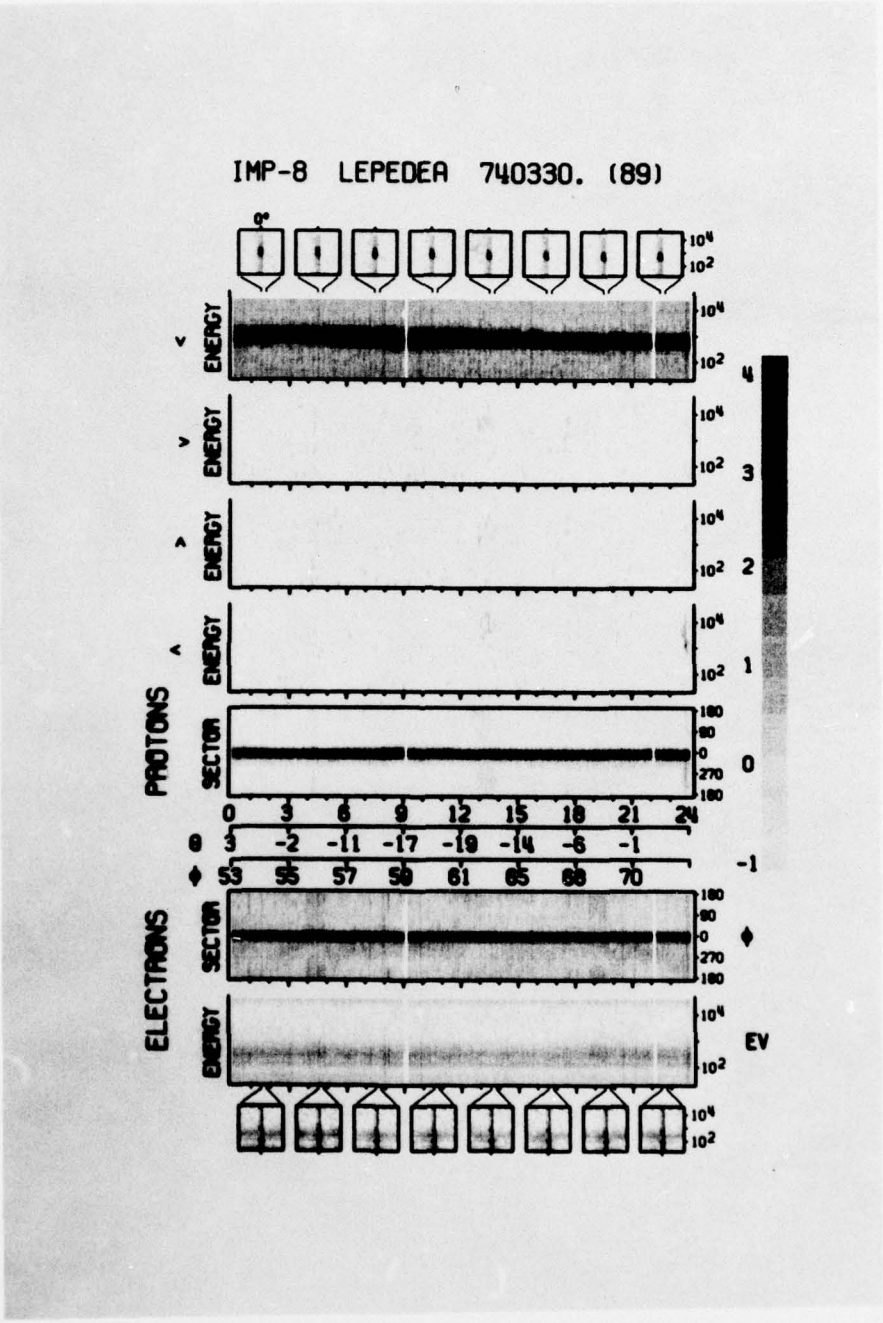
IMP-8 LEPEDEA 740330. (89)
0°
PROTONS
ELECTRONS
ENERGY
SECTOR
0 3 6 9 12 15 18 21 24
3 -2 -11 -17 -19 -14 -6 -1
53 55 57 59 61 65 68 70
EV

Plate 2

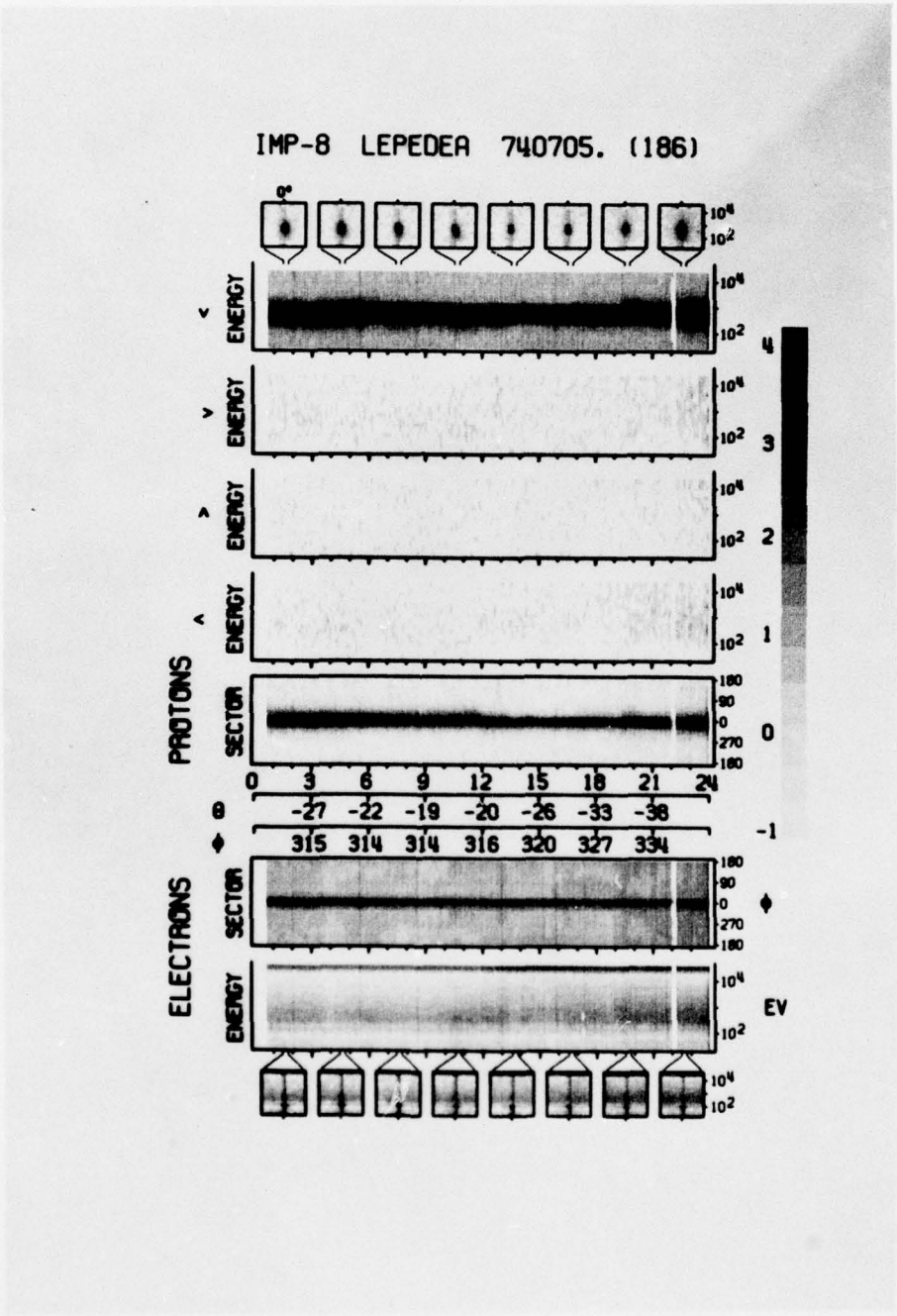
IMP-8 LEPEDEA 740705. (186)
PROTONS
ELECTRONS
ENERGY
SECTOR
EV
0 3 6 9 12 15 18 21 24
-27 -22 -19 -20 -26 -33 -38
315 314 314 316 320 327 334

Plate 3